AL/HR-TR-1996-0040

SMOOTH EYE MOVEMENT RESPONSE TO COMPLEX MOTION SEQUENCES

Julie Mapes Lindholm
Paul A. Wetzel
Timothy M. Askins

Hughes Training, Inc., Training Operations
6001 S. Power Road, Bldg. 561
Mesa, AZ 85206-0904

DTIC QUALITY INSPECTED 4

HUMAN RESOURCES DIRECTORATE
AIRCREW TRAINING RESEARCH DIVISION
6001 S. Power Road, Bldg. 558
Mesa, AZ 85206-0904

September 1996

Final Technical Report for Period June 1991 - June 1995

AIR FORCE MATERIEL COMMAND
BROOKS AIR FORCE BASE, TEXAS

19961223 054

ARMSTRONG LABORATORY

NOTICES

When Government drawings, specifications, or other data are used for any purpose other than in connection with a definitely Government-related procurement, the United States Government incurs no responsibility or any obligation whatsoever. The fact that the Government may have formulated or in any way supplied the said drawings, specifications, or other data, is not to be regarded by implication, or otherwise in any manner construed, as licensing the holder, or any other person or corporation; or as conveying any rights or permission to manufacture, use, or sell any patented invention that may in any way be related thereto.

The Office of Public Affairs has reviewed this report, and it is releasable to the National Technical Information Service, where it will be available to the general public, including foreign nationals.

This report has been reviewed and is approved for publication.

BYRON J. PIERCE
Project Scientist
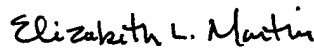
ELIZABETH L. MARTIN
Technical Director

LYNN A. CARROLL, Colonel, USAF
Chief, Aircrew Training Research Division

REPORT DOCUMENTATION PAGE

1. AGENCY USE ONLY (Leave blank)	2. REPORT DATE September 1996	3. REPORT TYPE AND DATES COVERED Final - June 1991 to June 1995

4. TITLE AND SUBTITLE

Smooth Eye Movement Response to Complex Motion Sequences

5. FUNDING NUMBERS

C - F41624-95-C-5011
PE - 62205F
PR - 1123
TA - B2
WU - 06

6. AUTHOR(S)
Julie Mapes Lindholm
Paul A. Wetzel
Timothy M. Askins

7. PERFORMING ORGANIZATION NAME(S) AND ADDRESS(ES)

Hughes Training, Inc.
Training Operations
6001 South Power Road, Bldg. 561
Mesa, AZ 85206-0904

8. PERFORMING ORGANIZATION REPORT NUMBER

AL/HR-TR-1996-0040

9. SPONSORING/MONITORING AGENCY NAME(S) AND ADDRESS(ES)

Armstrong Laboratory
Human Resources Directorate
Aircrew Training Research Division
6001 South Power Road, Bldg. 558
Mesa, AZ 85206-0904

10. SPONSORING/MONITORING AGENCY REPORT NUMBER

11. SUPPLEMENTARY NOTES

Armstrong Laboratory Technical Monitor: Dr. Elizabeth L. Martin (602) 988-6561

12a. DISTRIBUTION/AVAILABILITY STATEMENT

Approved for public release; distribution is unlimited.

12b. DISTRIBUTION CODE

13. ABSTRACT *(Maximum 200 words)*

To examine the spatiotemporal properties of the motion sensors for the smooth pursuit system, we presented horizontal motion sequences in which successive target displacements were in accord with a composited waveform representing the sum of a constant velocity ramp and a sawtooth. The sequences differed in global velocity (GV = ramp velocity = 0 or 4 deg/sec), local velocity (LV = ramp velocity + sawtooth velocity = -8 or -4 deg/sec, for GV = 0, and -8, -4, 0, 8, 12 deg/sec, for GV = 4), and local-segment duration (12 values between 67 and 700 msec). When the duration of a local-velocity segment was relatively short ($\leq$ 133 msec, for GV = 4 deg/sec; $\leq$ 200 msec, For GV = 0 deg/sec), mean pursuit velocity matched the GV. As the segment duration increased, mean pursuit velocity shifted gradually toward the LV. Changes in cumulative saccadic amplitude mirrored the changes in smooth pursuit velocity. The spatiotemporal-frequency spectra of the motion sequences suggested that the pursuit system responded in accord with the drift velocities of very low spatial frequencies. The spectra of the space-time retinal images suggested that pursuit was maintained not by the absence of retinal image motion but by the presence of appreciable spectral energy for components with a drift velocity of approximately zero.

14. SUBJECT TERMS
Efference copy; Eye movements; Fourier transform; Motion sensors; Retinal images; Retinal velocity error; Saccadic eye movements; Smooth pursuit eye movements; Spatiotemporal frequency

15. NUMBER OF PAGES
41

16. PRICE CODE

17. SECURITY CLASSIFICATION OF REPORT	18. SECURITY CLASSIFICATION OF THIS PAGE	19. SECURITY CLASSIFICATION OF ABSTRACT	20. LIMITATION OF ABSTRACT
Unclassified	Unclassified	Unclassified	UL

CONTENTS

List of Figures

PREFACE

SMOOTH EYE MOVEMENT RESPONSE TO COMPLEX MOTION SEQUENCES

INTRODUCTION

Eye movements are typically categorized in terms of their speed, the type of stimulus, and the "goal" of the eye-movement system. *Smooth pursuit eye movements* are relatively slow and occur when an observer attempts to track a small target moving in the visual field. It is generally accepted that the purpose of smooth pursuit is to keep the image of the target near or on the fovea and to reduce the speed at which the target's image moves across the retina. Thus, accurate tracking of a target facilitates perception of its spatial form, both by positioning the target's image on the area of the retina with the highest visual acuity and by reducing the speed of that image.

The spatial resolution of a flight simulator's visual system is usually much less than that of the fovea. Therefore, the details (high spatial frequencies) of a target are not represented in the display image, and accurate tracking of a target may not enhance target perception. To reduce this problem, a few simulation systems track head and eye movements and use that information to position a high resolution *area of interest* (AOI) within the display image. Optimal positioning of the AOI requires an algorithm that can accurately predict future direction of gaze. Clearly, a better understanding of the pursuit system would improve such prediction. It might also support the development of "intelligent" image generation systems which could, for example, selectively vary spatial or temporal resolution in order to elicit tracking of a given target or to optimize the representations of targets that are likely to be tracked.

In prior studies of smooth pursuit, the target has typically moved along a simple, predictable trajectory. With target position plotted as a function of time, common waveforms include a *ramp* (constant-velocity motion); a *step-ramp* (abrupt change in position followed by constant-velocity motion); a *sawtooth* (periodic abrupt change in position followed by constant-velocity motion); a *triangle* (constant-velocity motion in one direction followed by constant-velocity motion in the opposite direction); and a *sinusoid* (sinusoidally varying velocity, with the speed decreasing to zero before a change in direction). Smooth pursuit has also been tested with pseudorandom trajectories representing a sum of sinusoids or bandlimited white noise. Pursuit performance is usually measured in terms of gain (eye velocity/stimulus velocity or, for sinusoidal motion, eye amplitude/target amplitude). Gain has been shown to be affected by several parameters of target motion, such as velocity (Collewijn & Tamminga, 1984) and acceleration (Lisberger, Evinger, Johanson & Fuchs, 1981), as well as by nonvisual factors such as expectations (Kowler, 1989).

The smooth-pursuit system is often viewed as a control system featuring a negative and a positive feedback loop (Hallet, 1986; Leigh & Zee, 1991; Lisberger, Morris, & Tychsen, 1987; Robinson, Gordon, & Gordon, 1986; Young, 1971). Figure 1 depicts a typical, if simplified, model of this type. In this model, the stimulus for smooth pursuit is taken to be velocity (as opposed to acceleration or position), nonvisual influences and system limitations are disregarded, and the head is assumed to be stabilized. A retinal velocity error is obtained by subtracting the

eye velocity from the target velocity. The retinal velocity error is added to a copy of the pursuit command (efference copy), providing a reconstruction of the original target-velocity signal. This signal drives the pursuit system. Thus, if the eyes are stationary, the retinal velocity error will stimulate the pursuit system. If a moving target is being tracked accurately, the retinal error signal will be reduced to zero and the efference copy will cause pursuit to continue. It follows then that if the target is not moving, but nonetheless remains stationary (if intermittent) on the retina while the eyes are engaged in smooth pursuit, the system will respond by maintaining that pursuit. This is the situation for "sigma motion" and related phenomena (Heywood, 1973; Stoper, 1973; Lamontagne, Desjardins & Pivik, 1993).
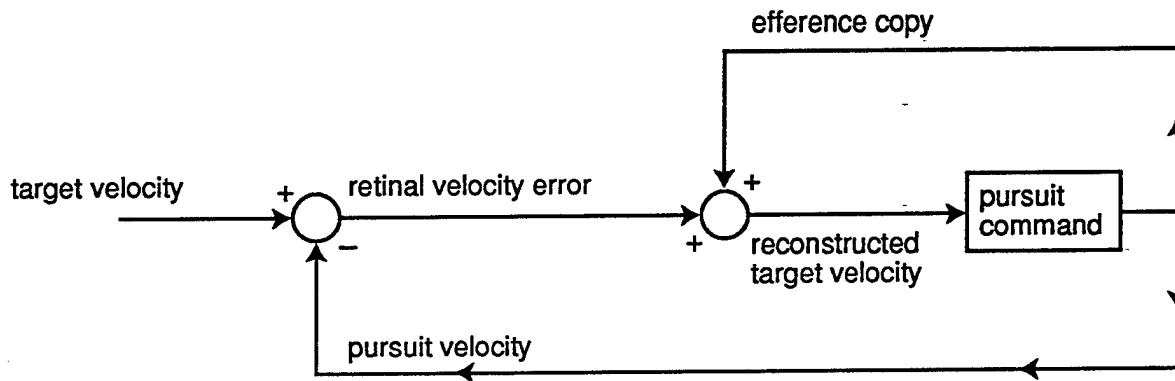
Figure 1
Typical Model of the Smooth Pursuit Eye Movement System

The term *retinal velocity error* is sometimes defined as the difference between eye and target velocity. The term is also used to refer to the velocity signal extracted from the spatiotemporal pattern of light on the retina by direction-selective cortical cells. The two are not necessarily equivalent. Moreover, the velocity signals for the pursuit system may be the same as those for the perceptual system, but they cannot be assumed to be so. In the following discussion, we will use the term *retinal image motion* to refer to variation over time in the retinal locus of the target's image and the term *velocity signal* to refer to the output of the relevant motion sensors. Our primary interest is in the features of the time-varying retinal image that account for the effective velocity signal.

Smooth pursuit eye movements are routinely elicited by temporally sampled motion rather than by continuous motion. Moreover, for a target following a triangular trajectory, Morgan and Turnbull (1978) found smooth tracking for sampling intervals that were too long (150 msec) to support perceived continuity. Thus, it appears that the neural mechanisms that provide input to the smooth pursuit system can extract a constant velocity signal from relatively infrequent samples of constant velocity motion. Once the velocity of smooth pursuit is well matched to the velocity represented by such a motion sequence, the retinal locus of the target's image will be approximately constant and, according to the model depicted in Figure 1, efference copy will cause that pursuit velocity to be maintained.

2

Hempstead (1966) examined form and motion perception during attempts to track a target following a staircase trajectory: Successive horizontal displacements of the target were in accord with a velocity of zero for $k - 1$ and a velocity of kv for 1 out of every k presentations (for $k = 2$ and 4). He reported that if the observer fixated a stationary spot on the screen, the perceived motion was not continuous. In contrast, during tracking instructions, a multiline target appeared to move continuously across the display. Hempstead proposed that tracking was in accord with velocity v (see also Lindholm 1992a,b).

A staircase is a composite waveform representing the sum of a constant velocity ramp and a sawtooth. In Hempstead's study, the velocity v corresponded to the velocity specified by the ramp. Although Hempstead did not record eye movements, we have confirmed that some staircase trajectories elicit pursuit eye movements in accord with the ramp velocity (Lindholm, 1991). This suggests that the pursuit system extracts a constant velocity signal when the intervals between samples of constant velocity motion are filled with multiple presentations of the target at the last sampled location. In addition, it means that a constant pursuit velocity is maintained in spite of the fact that retinal image motion persists. The question, then, is twofold: For staircase motion, why is the velocity signal seemingly in accord with the ramp rather than the composite waveform, and why is the pursuit velocity maintained even though retinal image motion is not reduced to zero?

A similar failure to follow high frequency waveforms was reported by Martins, Kowler, and Palmer (1985). They found poor pursuit of targets undergoing small-amplitude (≤ 30 arc min) sinusoidal motion when the frequency of the sinusoid was 1 Hz or greater, despite relatively low velocities and accelerations. When the frequency of the sinusoid was 4 Hz, they report that smooth pursuit occurred only during the "initial seconds" of a trial, after which the eye position records were comparable to those observed when the target was stationary. Martins et al. argue that the failure to track high frequency oscillations is not the result of motor limitations but "is likely to arise from slow processing of information about changes in the direction of retinal motion or from the inability to change expectations quickly about the direction of future motion" (Martins et al., 1985, p. 241).

The results of Martins et al. can be viewed as merely a failure of the pursuit system to respond to high frequency sinusoidal motion. However, if the sinusoidal trajectories are taken as the sum of a sinusoid and a zero-velocity "ramp," then their results suggest that the pursuit system responded in accord with the velocity specified by the ramp when the frequency of the sinusoid was high.

Regardless of the interpretation of the Martins et al. study, clearly some target trajectories that can be decomposed into a constant velocity ramp and a high frequency waveform elicit smooth pursuit in accord with the ramp. If the discrepancy between eye motion and target motion does not result from motor limitations, then it presumably arises from the velocity signal extracted by the motion sensors. Composite waveforms of this type therefore offer a useful tool for examining the spatiotemporal properties of these sensors.

In the experiment reported here, we recorded eye movements for observers attempting to track a target moving in accord with a variety of composite waveforms, each of which represented the sum of a constant velocity ramp and a sawtooth. These motion sequences were all characterized by speeds known to elicit good pursuit (Leigh & Zee, 1991). To assess whether the addition of a nonzero constant-velocity ramp has any appreciable effect on the response of the oculomotor system to a sawtooth waveform, we presented a ramp with a velocity of 0 deg/sec as well as one with a velocity of 4 deg/sec. We varied the period, direction, and speed of sawtooth motion. By so doing, we varied both the interval between samples of the constant velocity ramp and the velocity of the target during those intervals.

METHOD

Observers

Three Armstrong Laboratory employees (2 males, 1 female) served as observers. Two of the three (TB and DS) were emmetropic; the third (KAK) was myopic and wore corrective contact lenses. TB and KAK were in their twenties; DS was 41 years old.

Several months earlier, TB and KAK had served as observers in experimental sessions in which eye movements were measured for a subset of the stimuli used in the present experiment as well as for a number of related motion sequences. Observer DS had not previously participated in eye-recording sessions.

Apparatus

A Silicon Graphics IRIS 4D/80GT workstation was programmed to generate the stimuli and to control the timing and sequencing of the experimental sessions. By the use of double-buffering, the displayable graphics memory was modified only during the intervals between vertical scans; by appropriate setting of priorities, the UNIX operating system was prevented from interrupting a motion sequence. Tests were conducted to ensure that the IRIS consistently maintained the specified 60-Hz update rate.

The horizontal position of the left eye was measured by means of a custom-designed eye-position monitor that used an infrared reflectance technique to sense the iris-sclera borders. The analog signal was subjected to a first-order lowpass filter with a 100-Hz break frequency before being sampled by a 12-bit, Data Translation analog-to-digital converter (ADC). The ADC was mounted in an Everex 386/25 PC, which was connected to the IRIS by a serial line. For the calibration procedure, a signal from the experimenter caused the Everex to initiate sampling by setting the ADC's internal trigger. For the motion sequences, a pulse originating from a phototransistor mounted on the face of the CRT set the ADC's external trigger. In both cases, the eye-position signal was sampled at 600 Hz.

The stimuli were displayed on a high-resolution (1280 horizontal x 1024 vertical), 60 Hz, noninterlaced, RGB Hitachi Monitor. The width of the display raster was 34 cm. From the viewing distance of 90 cm, the interval between pixel centers subtended a visual angle of 1 arc

min. The front of the monitor was enclosed in a black, three-sided, cardboard box with a 37 cm x 18 cm opening. The box served to mask both the monitor frame and the phototransistor (used to trigger the ADC), which was attached to the lower left-hand corner of the display area.

The observer sat in a small booth that consisted of a metal frame covered with a heavy black cloth. The eye position monitor and a head and chin rest were mounted on a sturdy table. A three-button computer mouse and a computer joy stick were provided for observer and experimenter input, respectively.

Calibration of Eye-Position Monitor

The infrared emitter and detectors of the eye-position monitor were manually aligned at the beginning of each eye-recording session. Then, during an initial rough calibration, the observer was instructed to shift his or her gaze between three 21 x 21 pixel fixation crosses which were positioned in the center and on the far left and right edges of the display. Gain and balance controls were adjusted to ensure that these excursions produced a signal of approximately ±8 volts.

The experimenter initiated a computer-controlled calibration sequence prior to each trial. A 21 x 21 pixel fixation cross served as the target for this procedure. Following an initial presentation in the center of the display, the target was displaced to the right in four steps of 157 pixels (approximately 2.6 deg). It then returned to the center and was successively displaced to the left. The target was presented at each location for 1.5 sec. Eye position was continuously sampled throughout the 15-sec sequence.

The eye position data for the first center presentation were discarded. For each of the remaining nine positions, calibration statistics were based on the initial 125 msec (75 samples) of the last 500 msec of the 1500-msec presentation. A calibration was accepted only if it met two criteria: (a) the standard deviation of the 75 samples for each target position was less than 0.6% of the difference between the means for the farthest left and farthest right positions; and (b) the squared correlation between the nine eye-position means and the target-position values was greater than 0.998. The first criterion ensured that fixation was steady during the 125-msec period; the second criterion ensured that there was a linear relationship between measured eye position and target position. If these criteria were met, the slope and intercept values derived from a least squares linear regression were used to calibrate the eye-position data for the following trial.

Motion Sequences

The target was a short, "white," vertical line (1 x 11 pixels) centered vertically on a dark display. Its horizontal position varied over time in accord with a composite waveform formed by adding a constant velocity ramp and a sawtooth (Fig. 2). Each multisegment motion sequence was thus characterized by three velocities: the temporally global velocity (GV), defined by the ramp; the sawtooth velocity (STV), defined by the ramp of the sawtooth; and the temporally

5

Component Waveforms

Ramp

Sawtooth

Composite Waveforms

Continuous

Sampled
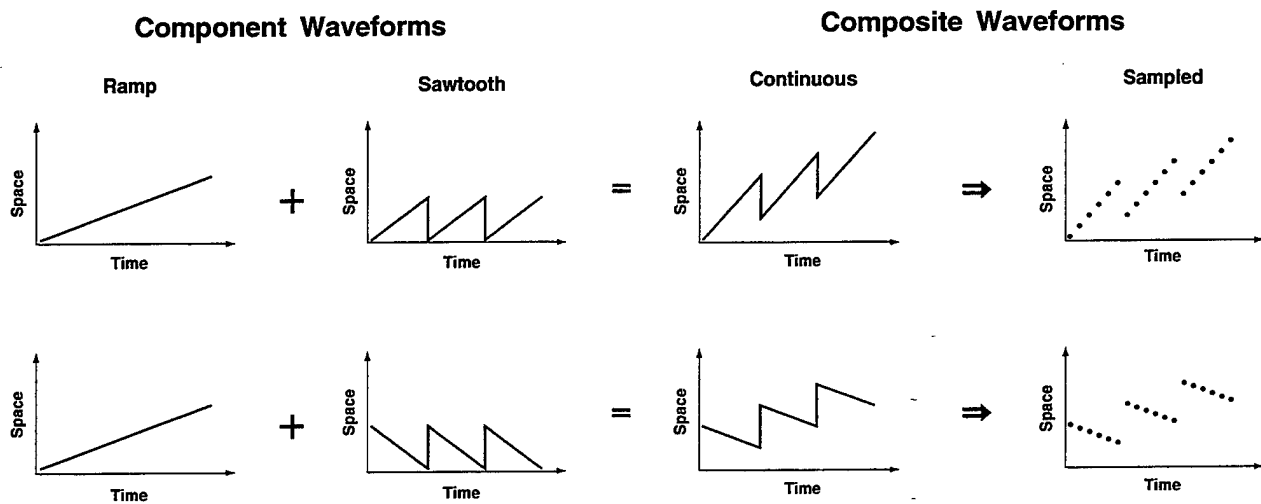
Figure 2

Examples of motion sequences created by summing a ramp and a sawtooth waveform. In the upper panels, the motion represented by the (ramp of the) sawtooth is in the same direction as that represented by the ramp; in the lower panels, the ramp and sawtooth motions are in opposite directions.

local velocity (LV) of a segment, defined by the ramp of the composite. The LV equaled the sum of the GV and the STV.

Sampled versions of 7 composite waveforms were presented, 2 with a GV of 0 deg/sec (GV0) and 5 with a GV of 4 deg/sec (GV4). The velocities characterizing these 7 conditions are summarized in Table 1. (Positive values indicate left-to-right motion.) Twelve local-motion segment durations were presented for each GV x LV condition: 67, 100, 133, 167, 200, 250, 300, 350, 400, 500, 600, and 700 msec (4, 6, 8, 10, 12, 15, 18, 21, 24, 30, 36, and 42 presentations of the target, with successive presentations separated by 16.7 msec).

For GV0, the location of the first target presentation for each local-motion segment was offset from the display center by one-half the segment path. Thus, regardless of the duration of a segment or the velocity of the target during that segment, the trajectory was always centered horizontally on the display. The trial duration for GV0 was set at 5.0 sec.

6

Table 1. *Motion Sequence Velocities*

Global (deg/sec)	Sawtooth (deg/sec)	Local (deg/sec)
0	-8	-8
0	-4	-4
4	-12	-8
4	-8	-4
4	-4	0
4	4	8
4	8	12

For GV4, left and right margins (offsets from the edge of the display raster) of 5 pixels were established to ensure that the full path of the target was visible through the opening of the box that masked the CRT frame. If the LV was positive or zero, the initial target position was on the left edge of the resulting display area. If the LV was negative, the initial target position was offset to the right so that the last position of the first segment fell on the left edge. Trial duration for a given trajectory was determined by the number of complete local motion segments that could be written across the 21.2-deg display. Before beginning each segment, the computer software calculated whether the initial target position (for the negative sawtooths) or the final target position (for the positive sawtooths) of the segment would extend beyond the maximum display position. If it would, the trial was terminated before initiating that segment. For GV4, then, the total trial duration varied from 3.5 to 5.3 sec. The shortest trial durations occurred for the motion sequences with high local speeds and long local segments.

Procedure

Each observer participated in a minimum of 21 experimental sessions, 3 for each of the 7 conditions. A different pseudo-random order of the 7 conditions was generated for each observer, with the restriction that each of the 7 conditions be presented once within each third of the experiment. Due to observer fatigue or repeated failure to meet calibration requirements, a few sessions were terminated before a full set of data had been gathered. The data for other trials were discarded due to eye blinks. Motion sequences for which data were missing or discarded were presented during the next scheduled session or in one or more extra, partial sessions at the end of the experiment.

A complete experimental session consisted of 3 blocks of 12 trials. The trials differed in segment duration. The order of presentation of the 12 durations was randomized independently for each block within a session. The first 2 blocks of trials served to familiarize the observer with the type of motion sequence. Eye position was recorded during the third block.

The experimenter aligned the eye-position monitor between the second and third blocks and then stayed in the subject booth until the end of the session. Each third-block trial was preceded by the computer-controlled calibration sequence. If the calibration criteria were not met, the calibration sequence was repeated. At the discretion of the experimenter, the position sensors were realigned following several calibration failures. A small flashlight was used when such an adjustment was required. Intertrial variation in the observer's level of dark adaptation was introduced by these adjustments as well as by the long durations (60-90 min) of a typical experimental session.

After an acceptable calibration, a fixation cross was presented for 2 sec in the center of the display. At the end of the following frame, a small rectangle presented at the bottom of the display (and masked from view) caused the ADC to begin sampling. The motion sequence began on the next frame. Eye position was sampled for 5 sec (3000 samples), regardless of the length of the motion sequence.

Head position was stabilized by a chin rest throughout the session. In addition, a dental biteboard and a forehead-restraining strap were used during the third block of trials. The observation booth was dark except for light emitted by a small shrouded lamp on the floor and stray light from the CRT and the eye-position monitor.

The observers viewed the stimuli binocularly. They were instructed to track the target throughout the trial and then, at the end of the trial, to push one of three buttons to classify their percept. (The perceptual data will be reported in a separate paper.) These instructions made it explicit that the perceived form and motion of the target could vary from trial to trial. No feedback was provided.

Data Reduction and Analysis

To ensure that the data were free of artifacts and blinks, a computer-generated display of each eye-position record was examined visually before it was processed. For each acceptable record, a 10-msec velocity estimate V was computed for each eye position sample, s, $3 < s < 2,998$, according to the formula $V_s = (P_{s+3} - P_{s-3})/(6/\text{sampling rate})$, where P is eye position. Saccades were detected by an algorithm employing both a velocity criterion and a duration criterion. The accuracy of the algorithm was checked by visual inspection of each eye-position record.

The time and amplitude of each saccade were stored for subsequent analyses. Velocity estimates identified as part of a saccade were removed from the original set of 2,994. All remaining values were considered to be measures of smooth pursuit.

Our goal was to characterize the oculomotor response after the visual system had fully processed the composite waveform and before the onset of any anticipatory end-of-trial effects. Ideally, in selecting the interval over which measures would be averaged, we would hold constant the main factors likely to affect system response: the time from trial onset, the duration of the interval, and the number of local segments preceding and included within the interval. Although the variation in segment duration

8

precluded this level of control, inspection of the eye records indicated that the oculomotor response for individual trials was typically well established after 1.0 to 1.5 sec. Moreover, the variability of smooth pursuit velocity within a segment appeared comparable to that between segments, and saccades were not tightly linked to segment onset. It thus seemed unlikely that systematic distortions would be introduced by summarizing the data over intervals that in some cases contained many segments and in other cases contained less than one segment.

In order to compute the desired summary response measures, we initially divided each 5-sec eye position record into bins of 500 msec and calculated the average smooth-pursuit velocity and the cumulative saccadic amplitude for each bin. The latter measure was obtained by summing the *signed* amplitudes of the saccades that began within the bin.

The data for the first three bins were discarded so that, in all cases, at least two full cycles of the composite waveform would have been presented prior to the assessment interval. Because some of the motion sequences had a duration of only 3.5 sec, the data for the last three bins were discarded. Preliminary analyses of variance (ANOVAs) of the mean velocities and cumulative saccadic amplitudes for Bins 4 to 7 indicated that the main effect of Bin and interactions involving Bin contributed relatively little variance to the data. Therefore, the velocity and saccadic measures were each averaged over the four bins for further analysis.

Univariate analyses of variance (ANOVA) were performed on the mean pursuit velocity and the cumulative saccadic amplitude measures for each GV. The three trials per observer per LV x duration combination were treated as replications. Thus, each of the four ANOVAs included four factors: observer, LV, segment duration, and replication. Both observer and replication were treated as random variables. Error terms were not pooled.

RESULTS

Representative records of eye and target position are presented in Figures 3-5. As Figure 3 illustrates, for segment durations less than about 167 msec, smooth pursuit velocity was in accord with the GV, and saccades were infrequent and of small amplitude. For segment durations of "intermediate" length, mean pursuit velocity shifted towards the LV, and saccades were more frequent and of higher amplitude (see Fig. 4). For the longest segment durations, mean pursuit velocity approached the LV, and saccades were of high amplitude (see Fig. 5). Note (in Figs. 4 and 5) that saccades were not consistently linked to the end of a sawtooth period and that, concomitantly, the periods of saccade-free smooth pursuit varied in duration. Saccades were, however, usually in the direction of the sawtooth step.

The results of the ANOVAs indicated that LV, segment duration, observer, and the interactions of these factors had significant effects on mean pursuit velocity and mean cumulative saccadic amplitude. With the exception of the main effects of LV for GV0 ($F_{1,2} = 9.41$, $p > .05$ and $F_{1,2} = 7.65$, $p > .10$, for the pursuit and saccade measures, respectively), the main effects (observer, LV, duration) and first-order interactions (LV x duration; observer x LV; and observer x duration) were all significant ($p < .0001$ in most cases) in each of the four analyses. In addition, the observer x LV x duration interactions were both significant for GV4.

tb
GV = 4 deg/s
LV = -8 deg/s
Dur = 167 ms

ds
GV = 0 deg/s
LV = -8 deg/s
Dur = 167 ms

kak
GV = 4 deg/s
LV = 12 deg/s
Dur = 167 ms

kak
GV = 4 deg/s
LV = 0 deg/s
Dur = 167 ms
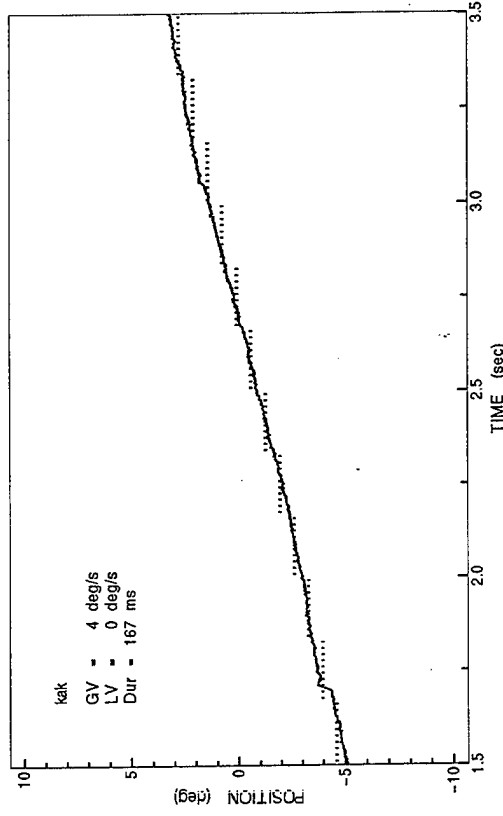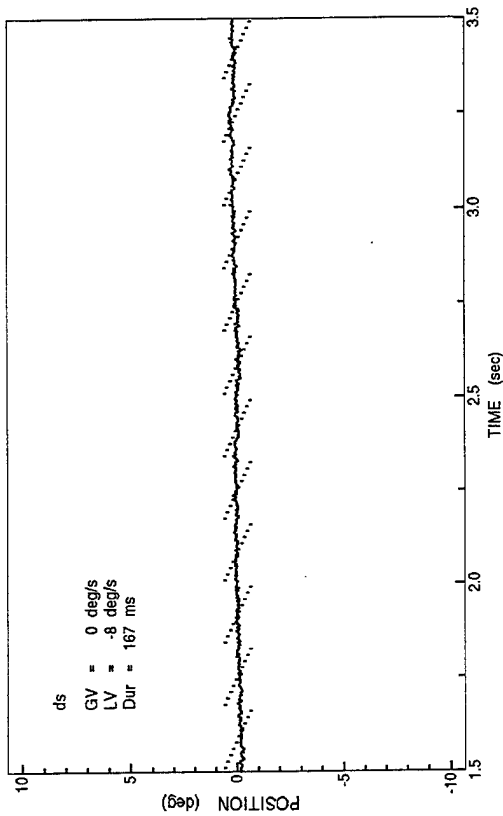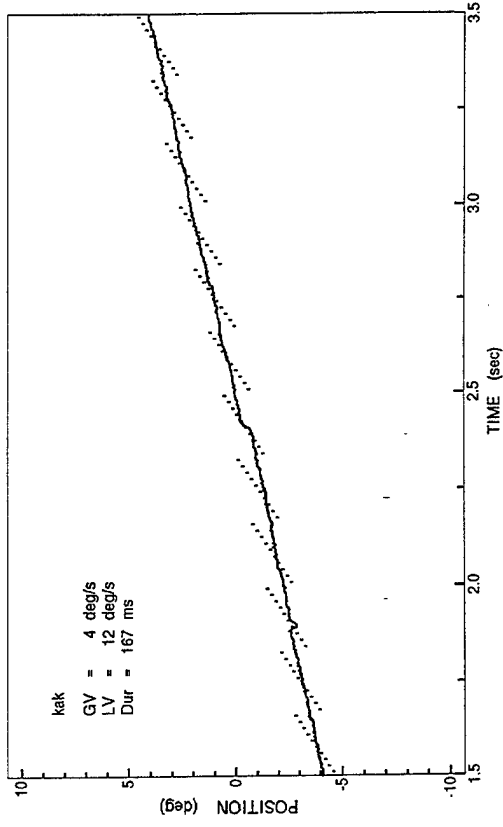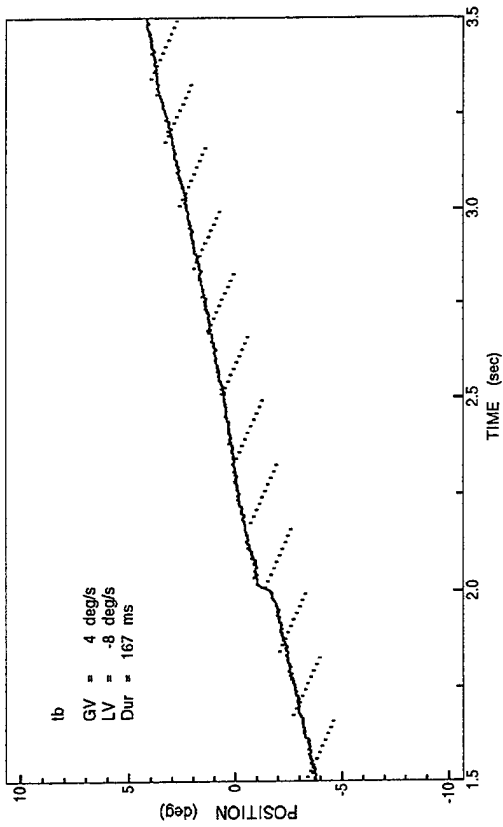
Figure 3

Eye movement records for horizontal motion sequences characterized by a global velocity (GV) and a local velocity (LV), with a local segment duration (Dur) of 167 msec. Target position is indicated by the dots. Minus values on the ordinate represent spatial locations to the left of center.

10
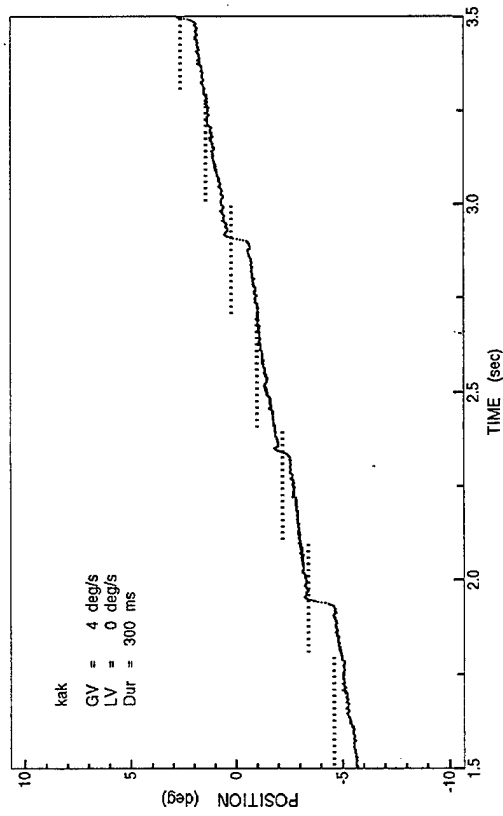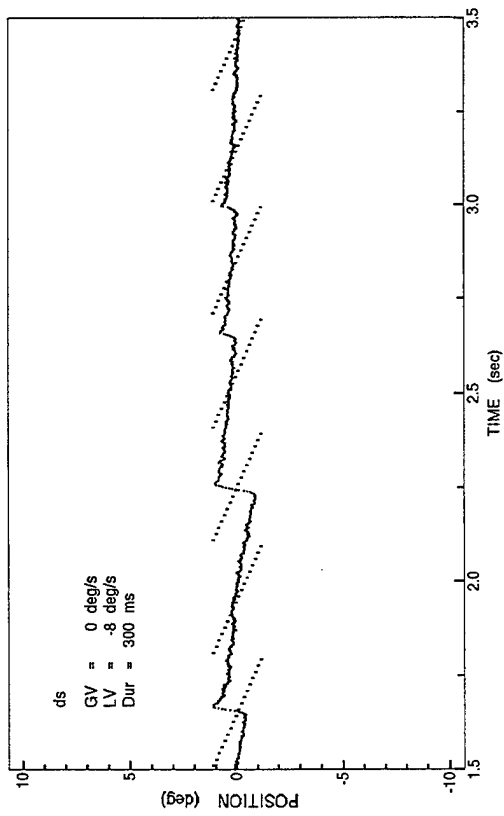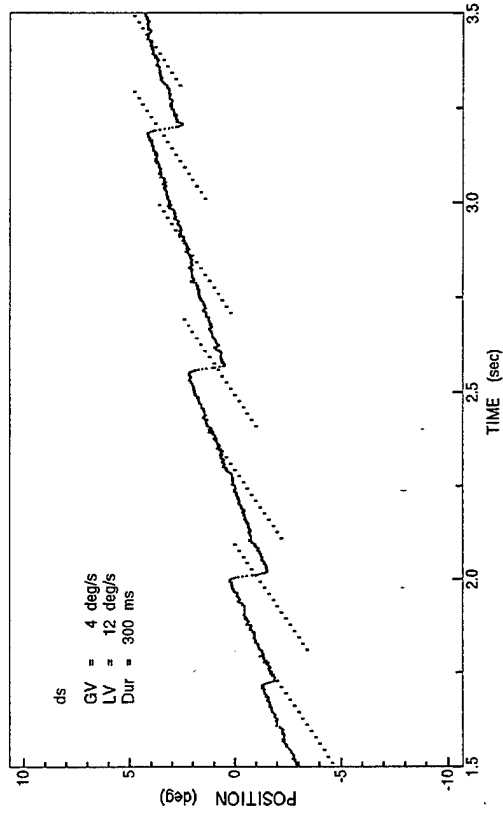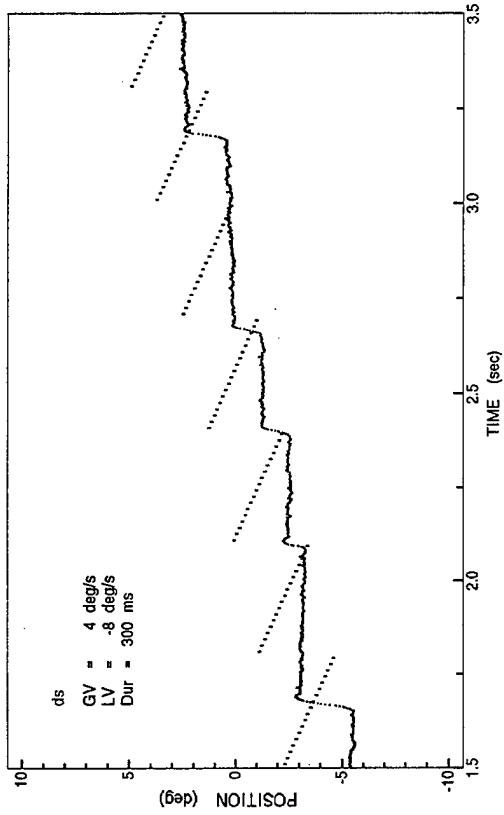
Figure 4

Eye movement records for horizontal motion sequences characterized by a global velocity (GV) and a local velocity (LV), with a local segment duration (Dur) of 300 msec. Target position is indicated by the dots. Minus values on the ordinate represent spatial locations to the left of center.
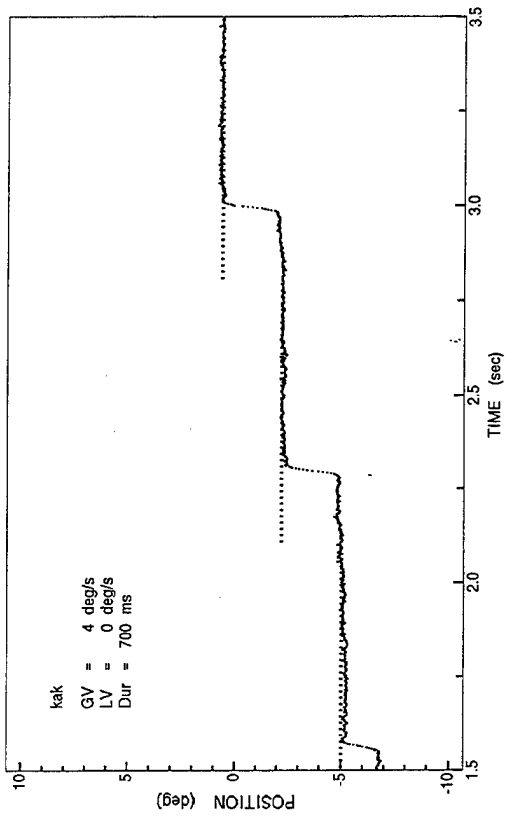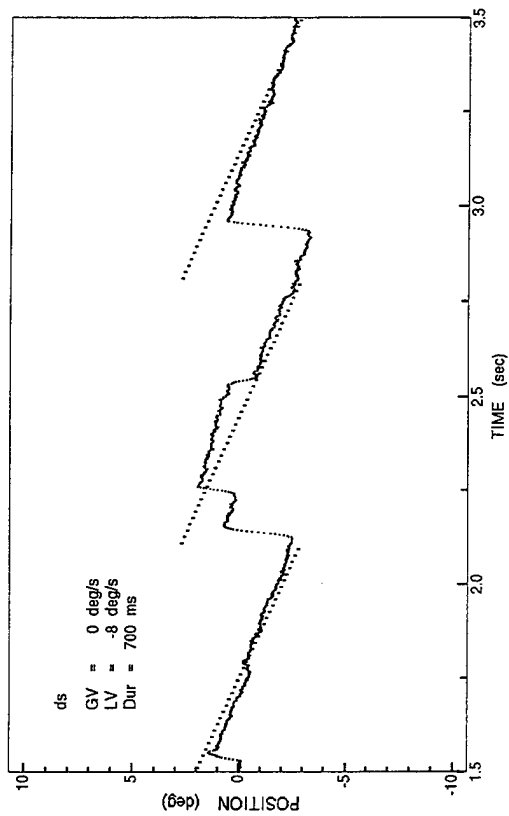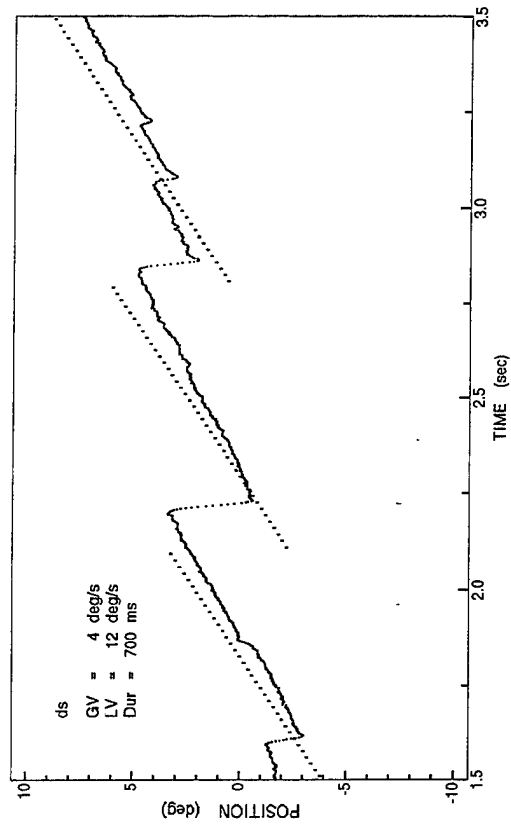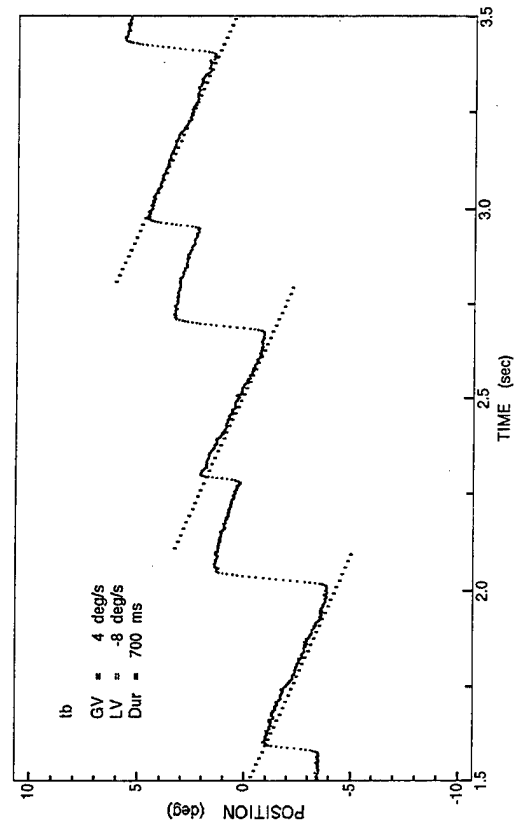
Figure 5

Eye movement records for horizontal motion sequences characterized by a global velocity (GV) and a local velocity (LV), with a local segment duration (Dur) of 700 msec. Target position is indicated by the dots. Minus values on the ordinate represent spatial locations to the left of center.

12

The LV x duration interactions are show in Figure 6, where group mean pursuit velocity (upper panels) and cumulative saccadic amplitude (lower panels) are plotted as a function of segment duration for each of the seven conditions (GV0, left panels; GV4, right panels). The general pattern of results is clear: For the shortest segment durations, mean pursuit velocity was in good agreement with the GV and cumulative saccadic amplitude was approximately 0 deg/sec. As segment duration increased, mean pursuit velocity shifted from the GV toward the LV, and mean cumulative saccadic amplitude shifted from zero toward the cumulative amplitude of the *sawtooth* step (in deg/sec).[1]

When the GV was 0 deg/sec, the mean pursuit velocities (Fig. 6, upper left panel) for both LV = -4 and LV = -8 were approximately 0 deg/sec (-0.11 to 0.06 deg/sec) for segment durations ≤ 200 msec. Mean pursuit velocities were slightly below zero (-0.58 and -0.86 deg/sec for LV = -4 and -8 deg/sec, respectively) for a segment duration of 250 msec and continued to decline out to a segment duration of 700 msec. Pursuit speed for LV = -8 deg/sec was roughly twice that for LV = -4 deg/sec for segment durations ≥ 300 msec.

The pattern of results for the measure of cumulative saccadic amplitude (Fig. 6, lower left panel) is highly similar to the pattern for pursuit velocity. For segment durations ≤ 200 msec, mean amplitudes were approximately 0 deg/sec. The LV = -4 and LV = -8 means were both above zero for a segment duration of 250 msec, and they became increasingly positive, with a ratio of about 2:1, as the segment duration increased to 700 msec.

When the GV was 4 deg/sec (Fig. 6, right panels), the mean pursuit velocities for segment durations ≤ 133 msec were well matched to the GV for all 5 LVs. The average pursuit velocities for the two positive and three negative sawtooths differed by 0.87 deg/sec for a segment duration of 167 msec. This difference increased to 1.98 deg/sec for a segment duration of 200 msec. As segment duration increased from 200 to 700 msec, the means shifted progressively toward the LVs of the motion sequences.

The mean cumulative saccadic amplitudes for the motion sequences with a GV of 4 deg/sec (Fig. 6, lower right panel) roughly mirrored the mean smooth pursuit velocities, except that they diverged from a baseline amplitude of 0 deg/sec rather than a baseline velocity of 4 deg/sec. In particular, this measure first showed an effect of the sawtooth waveform for a segment duration of 167 msec, after which the magnitude of the effect increased with duration.

To test the statistical significance of the difference between GV0 and GV4 in the segment durations for which effects of the sawtooth were first apparent, ANOVAs were conducted on the mean pursuit velocities for the 5 lowest segment durations (67 - 200 msec) for each of the LVs for GV0 and

---

[1] If the motion had been continuous, each sawtooth step would have equaled minus the product of the STV and the segment duration. Multiplying this value by f_{st}, the sawtooth frequency in cycles/sec, would give the cumulative amplitude of the sawtooth step, in deg/sec. It would be equal to minus the STV, regardless of the duration of a sawtooth-defined segment. For our sampled-motion sequences, however, the last position within a segment was not displayed, and the last displayed position in segment n was separated from the first position in segment $n + 1$ by Δt. The size of a sawtooth step was therefore reduced by Δt (STV + GV)-- that is, by $\Delta t \cdot$ LV. As a result, the cumulative amplitude of the sawtooth step, in degrees per second, equaled $-(STV - f_{st} \cdot \Delta t \cdot LV)$.

13
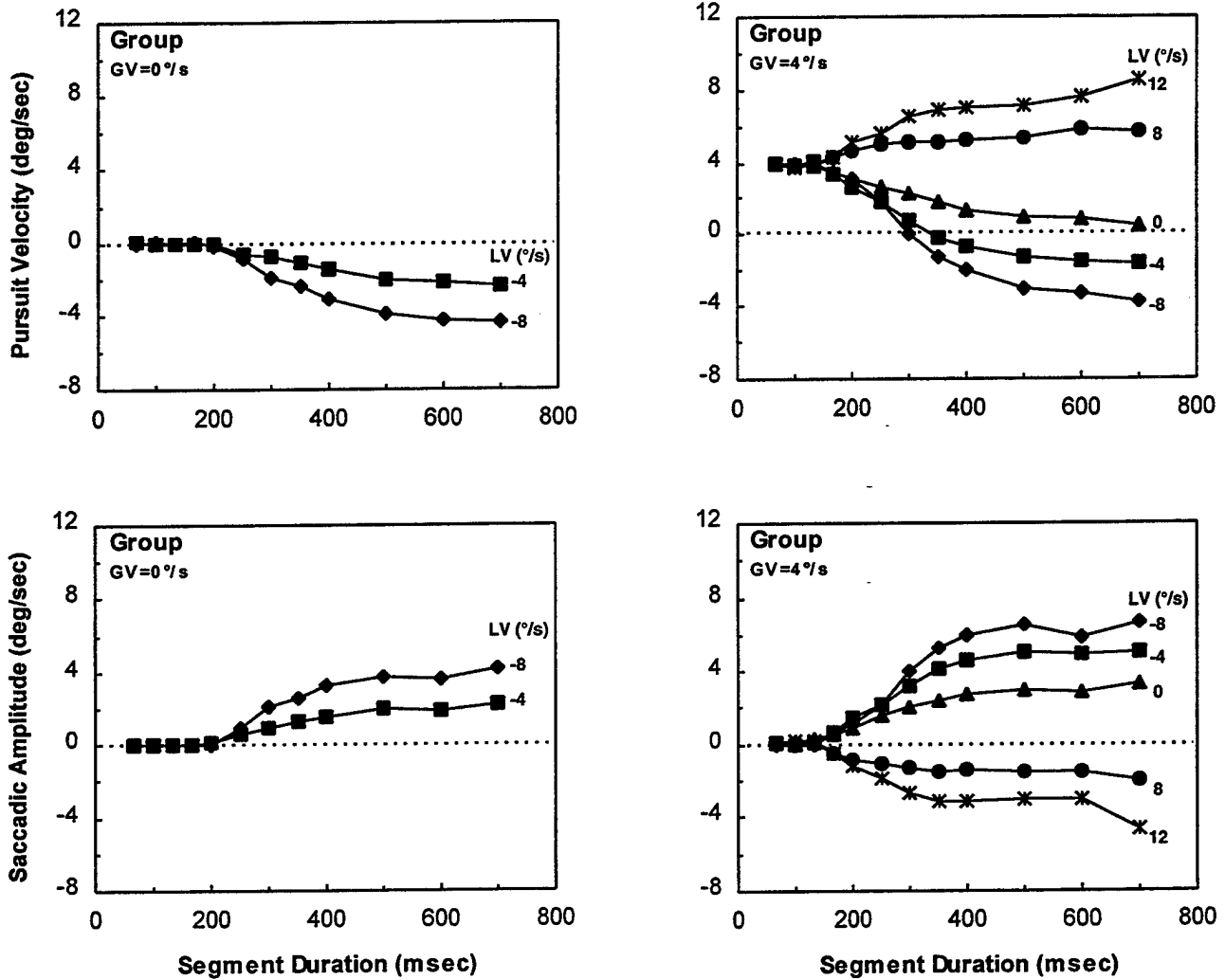
Figure 6

Group mean oculomotor responses to multisegment motion sequences characterized by a temporally global velocity (GV) and a temporally local velocity (LV). Pursuit velocity (upper panels) and cumulative saccadic amplitude (lower panels) are shown as a function of segment duration for each LV, for a GV of 0 deg/sec (left panels) and a GV of 4 deg/sec (right panels). Each data point represents the average of the response measures for 4 successive 500-msec periods, beginning 1.5 sec after onset of a motion sequence, for each of 3 trials for 3 observers. The pursuit-velocity for a given 500-msec period was itself the average of up to 300 measures.

14

for LV = -4, 0, 8, and 12 deg/sec for GV4. (The LV of -8 deg/sec was excluded from the GV4 analysis to limit the STVs to ± 4 and ± 8 deg/sec for both GVs.) The results support the previous description: The LV x duration interaction was significant ($F_{12,24}$ = 4.65, p < .001) in the GV4 analysis, whereas neither the duration nor the LV x duration interaction approached significance ($F_{4,8}$ = 2.12, p > .10 and $F_{4,8}$ = 0.82, respectively) in the GV0 analysis. This was true in spite of the fact that the observer x LV x duration interaction, which served as the error term for the LV x duration effect, was itself significant in the former but not in the latter analysis ($F_{24,120}$ = 3.92, p< .0001 and $F_{8,60}$ = 0.53, respectively).

Figures 7 - 9 illustrate the observer x LV x duration interactions for both GVs and response measures. (Recall that for GV4 this three-way interaction was statistically significant for both measures, whereas for GV0, only the observer x LV and observer x duration interactions were significant.) As inspection of these figures indicates, the basic pattern of results held over observers. For each, mean pursuit velocity was in accord with the GV for the shortest segment durations and shifted progressively toward the LV as segment duration increased. The shifts in cumulative saccadic amplitude paralleled those in pursuit velocity. The differences among observers were quantitative rather than qualitative.

Specifically, as shown in Figure 7, DS's response curves were very similar to the mean response curves for the 3 observers (Fig. 6). KAK's responses (Fig. 8) were relatively *un*affected by the *sawtooth* waveform. For GV0, her means for both measures were approximately 0 deg/sec until the segment duration was 400 or 500 msec (for LV = -8 and -4 deg/sec, respectively), whereas the means for the other two observers deviated from 0 deg/sec for segment durations greater than 200 ms. Moreover, KAK's mean pursuit speeds and saccadic amplitudes for the longest durations were less than those of the other two observers. For GV4, the segment durations at which she first showed effects of the sawtooth were shorter for the negative STVs (resulting in a decrease in pursuit velocity) than for positive STVs, and she showed little effect of speed in either direction. Finally, TB's oculomotor system seemed to "prefer" high speeds (Fig. 9). For the relatively long segment durations, his mean pursuit speeds and saccadic amplitudes were higher than those of the other two observers, and for GV4, the shift from GV tracking to composite-waveform tracking occurred at shorter segment durations for the positive sawtooths than for the negative sawtooths.

A somewhat different view of the accuracy of pursuit during a local motion segment is provided by Figure 10, where pursuit gain relative to the local velocity of the target (i.e., gain = pursuit velocity/ LV) is plotted as function of segment duration for the six conditions with a nonzero LV. Note that for observer DS (upper panels) and observer TB (lower panels), about the same level of gain was obtained for all six conditions. For observer KAK, gain for the longest segment duration varied substantially with the motion sequence velocities. In general, for this measure of gain, when the STV and the GV were in opposite directions, tracking accuracy never exceeded and was usually less than that when the component velocities were in the same direction.

We also assessed gain with respect to the sawtooth velocity (i.e., gain = [mean pursuit velocity - GV]/ STV). With that measure, gains for the longest segment durations tended to be highest for LV = 0 and lowest for the two positive sawtooths (i.e., for LV = 8 and 12 deg/sec).

15
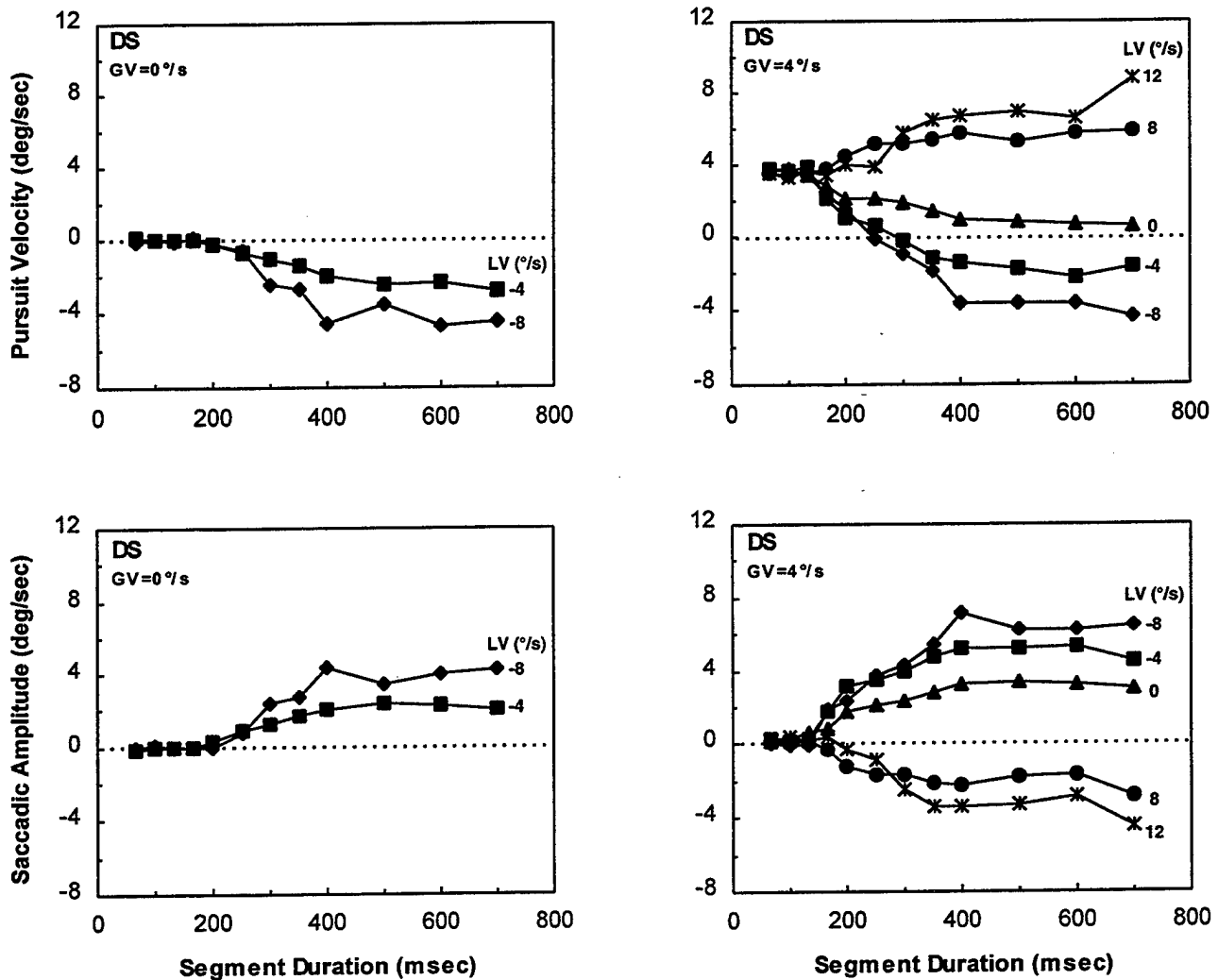
Figure 7

Mean oculomotor responses of observer DS to multisegment motion sequences characterized by a temporally global velocity (GV) and a temporally local velocity (LV). Pursuit velocity (upper panels) and cumulative saccadic amplitude (lower panels) are shown as a function of segment duration for each LV, for a GV of 0 deg/sec (left panels) and a GV of 4 deg/sec (right panels). Each data point represents the average of the response measures for 4 successive 500-msec periods, beginning 1.5 sec after onset of a motion sequence, for each of 3 trials. The pursuit-velocity for a given 500-msec period was itself the average of up to 300 measures.
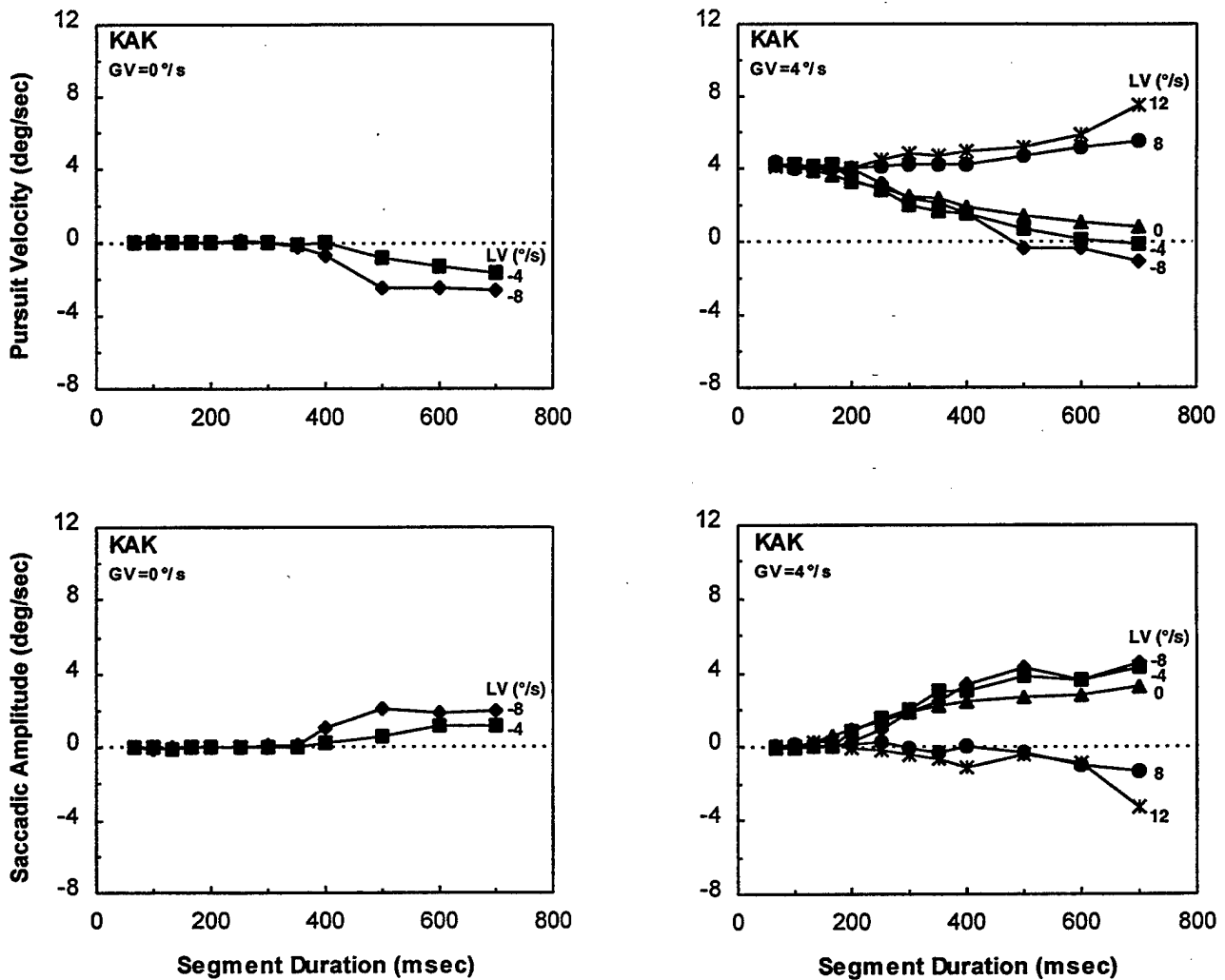
Figure 8

Mean oculomotor responses of observer KAK to multisegment motion sequences characterized by a temporally global velocity (GV) and a temporally local velocity (LV). Pursuit velocity (upper panels) and cumulative saccadic amplitude (lower panels) are shown as a function of segment duration for each LV, for a GV of 0 deg/sec (left panels) and a GV of 4 deg/sec (right panels). Each data point represents the average of the response measures for 4 successive 500-msec periods, beginning 1.5 sec after onset of a motion sequence, for each of 3 trials. The pursuit-velocity for a given 500-msec period was itself the average of up to 300 measures.
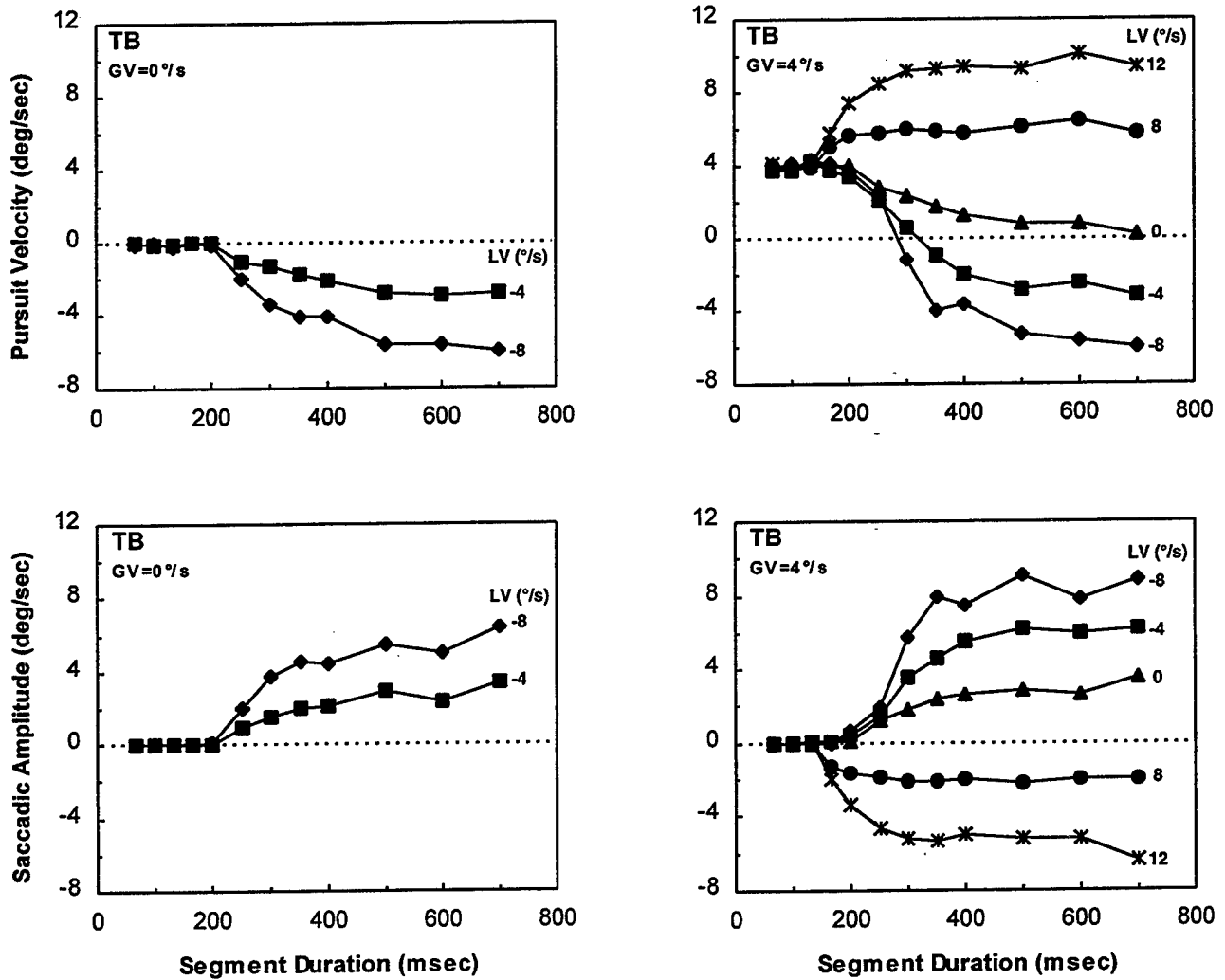
Figure 9

Mean oculomotor responses of observer TB to multisegment motion sequences characterized by a temporally global velocity (GV) and a temporally local velocity (LV). Pursuit velocity (upper panels) and cumulative saccadic amplitude (lower panels) are shown as a function of segment duration for each LV, for a GV of 0 deg/sec (left panels) and a GV of 4 deg/sec (right panels). Each data point represents the average of the response measures for 4 successive 500-msec periods, beginning 1.5 sec after onset of a motion sequence, for each of 3 trials. The pursuit velocity for a given 500-msec period was itself the average of up to 300 measures.
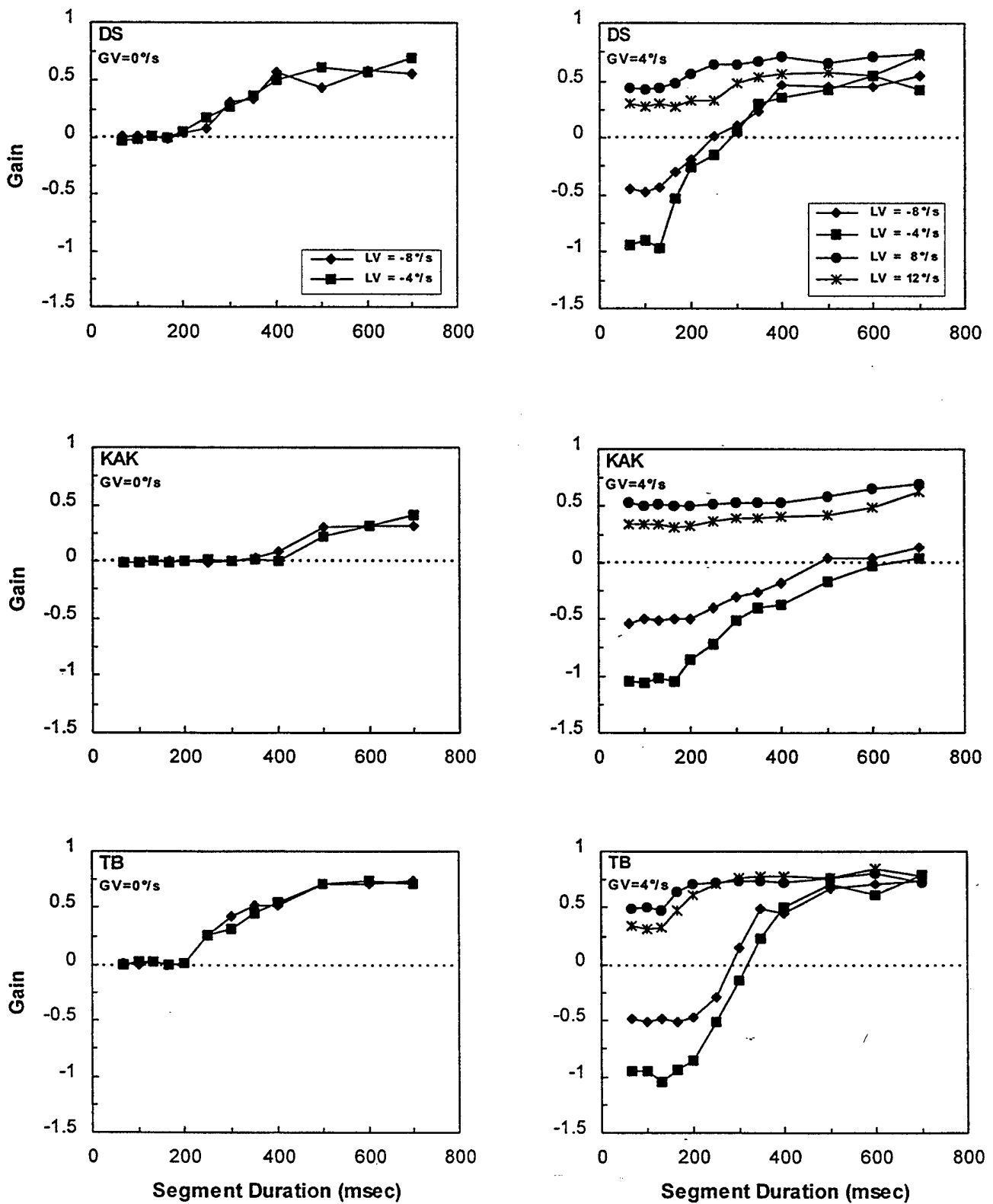
Figure 10

Mean gain, relative to the temporally local velocity (LV), for multisegment motion sequences with temporally global velocities (GV) of 0 deg/sec (left panels) and 4 deg/sec (right panels). Gain is plotted as a function of segment duration for each LV ≠ 0. Each data point represents the average gain for 4 successive 500-msec periods, beginning 1.5 sec after onset of a motion sequence, for each of 3 trials. The pursuit velocity for a given 500-msec period was itself the average of up to 300 measures.

19

DISCUSSION

The purpose of this experiment was to examine the spatiotemporal properties of the motion sensors for the smooth pursuit eye movement system. In an earlier study, Morgan & Turnbull (1978) demonstrated that the pursuit system could extract the constant velocity signal from motion sequences in which successive presentations of the target were separated in space by 27 arc min and in time by up to 150 msec. We found that, for similar spatial and temporal intervals, the pursuit system could extract the temporally global velocity from motion sequences in which the target was presented repetitively between successive samples of that velocity. (For a motion sequence with a GV of 4 deg/sec and a segment duration of 133 msec, corresponding points in successive segments were separated by 32 arc min.) The pursuit system could do this not only when the target was stationary between successive samples of the GV (i.e., when the spatiotemporal trajectory was a staircase), but also when the target was successively displaced, in accord with a constant temporally local velocity, during the GV-sampling interval. In the latter case, neither the direction nor the speed of motion between samples of the GV (i.e., during a local-velocity segment) had a consistent effect on pursuit velocity for motion sequences with a local-segment duration ≤ 133 msec. Thus, for such motion sequences, pursuit in accord with the GV was maintained despite the failure of smooth eye movements to reduce the retinal image motion to zero.

When the pursuit system responded in accord with the GV of a motion sequence, it necessarily failed to follow the temporally local motion. In good agreement with the research of Martins et al (1985), who found that the pursuit system showed little if any response to low-amplitude sinusoidal motion with frequencies of 4 to 5 Hz, we found no effect of local velocity for GV0 sequences with segment durations of up to 200 msec. Although this segment duration was longer than that (133 msec) supporting highly accurate GV tracking for the GV4 sequences, the similarity of the results for the two GVs suggests that the pursuit system was actively matching the GV of 0 deg/sec rather than merely failing to follow the LV.

It has been proposed that the analysis of motion in the retinal image begins with a spatiotemporal filtering process (Adelson & Bergen, 1985; van Santen & Sperling, 1984; Watson & Ahumada, 1985). If this view is correct, then an analysis of the spatiotemporal frequency spectra of our motion sequences may provide some insight into the basis of the velocity signal for the initiation of smooth pursuit as well as the characteristics of the retinal image necessary to maintain pursuit at a given velocity.

In Figure 2, the multisegment motion sequences were shown to represent sampled versions of composite waveforms constructed by summing two component waveforms: a constant velocity ramp and a sawtooth. Such sequences can also be constructed by convolving the space-time representation of a single local-motion sequence with a sampling function in which successive impulses are separated in time by the duration of the sequence and in space by the product of that duration and the GV (i.e., with a sampled version of the ramp). Because convolution in the space-time domain is equivalent to multiplication in the spatiotemporal-frequency domain, the Fourier transform of the space-time representation of a multisegment

motion sequence is the product of the transform of a single local-motion sequence and the transform of the sampling function.

Figures 11 and 12 illustrate this derivation of the spatiotemporal-frequency spectrum of a representative, multisegment motion sequence. In these and subsequent illustrations of amplitude spectra, the horizontal dimension represents horizontal spatial frequencies u from -30 cycles/deg to 30 cycles/deg, and the vertical dimension represents temporal frequencies w from - 30 Hz to 30 Hz. (Note that this orientation differs from that in Figs. 2 - 5). The brightness of a given point indicates its magnitude. Each pair of points symmetrically displaced from the origin represents a sinusoidal component with a drift velocity of $-w/u$.

To create these spectra, the lowpass spatial filtering of the CRT's electron spot was approximated in the space-time representation of a motion sequence: A low level of luminance (a digital value of 50) was assigned to one point on the left and to one point on the right of each target position (which had a digital value of 255). Consequently, in the motion-sequence spectra (but not in the sampling-function spectrum), magnitude is a decreasing function of spatial frequency, as it was in the space-time display images. Because a CRT does little temporal filtering, the bands of energy in the spectra should be understood to extend in the temporal frequency dimension well beyond the ± 30 Hz range that is depicted.

The spatiotemporal-frequency spectrum of a single 67-msec motion sequence with a velocity of -4 deg/sec is illustrated in the left panel of Figure 11. Several characteristics of the spectrum should be noted. First, the band of energy through the origin is in accord with the local velocity (i.e., its slope is 4), although there is considerable spread in both the spatial- and temporal-frequency dimensions and thus in the velocities of the individual components. (Spread in the w dimension is inversely proportional to the duration of the local motion sequence; spread in the u dimension is inversely proportional to the spatial extent of the sequence, which is roughly equal to the product of the segment duration and the LV). The side bands represent aliased frequencies. With a temporal sampling rate of 60 Hz, aliasing will occur for any component with $w \geq 30$ Hz. Note that the velocities of the aliased components differ substantially from the LV: All are drifting at the wrong speed; many are drifting in the opposite direction.

The right panel of Figure 11 illustrates the spectrum of a sampling function in which successive impulses are separated in time by 67 msec (the segment duration) and in space by 0.267 deg (i.e., duration · GV). The lines in this spectrum have a slope of -GV. They are separated in w by the temporal sampling rate (i.e., 1/0.067 sec = 15 Hz) and in u by the spatial sampling rate (i.e., 1/0.267 deg = 3.75 cycles/deg). Note that only the spatiotemporal frequency components that lie on the line through the origin are consistent with the GV of the motion sequence.

Figure 12 illustrates the spectrum of a multisegment motion sequence with a GV of 4 deg/sec, an LV of -4 deg/sec, and a segment duration of 67 msec. It represents the product of the spectra shown in Figure 11. In this spectrum, the components that fall on the line through the

21
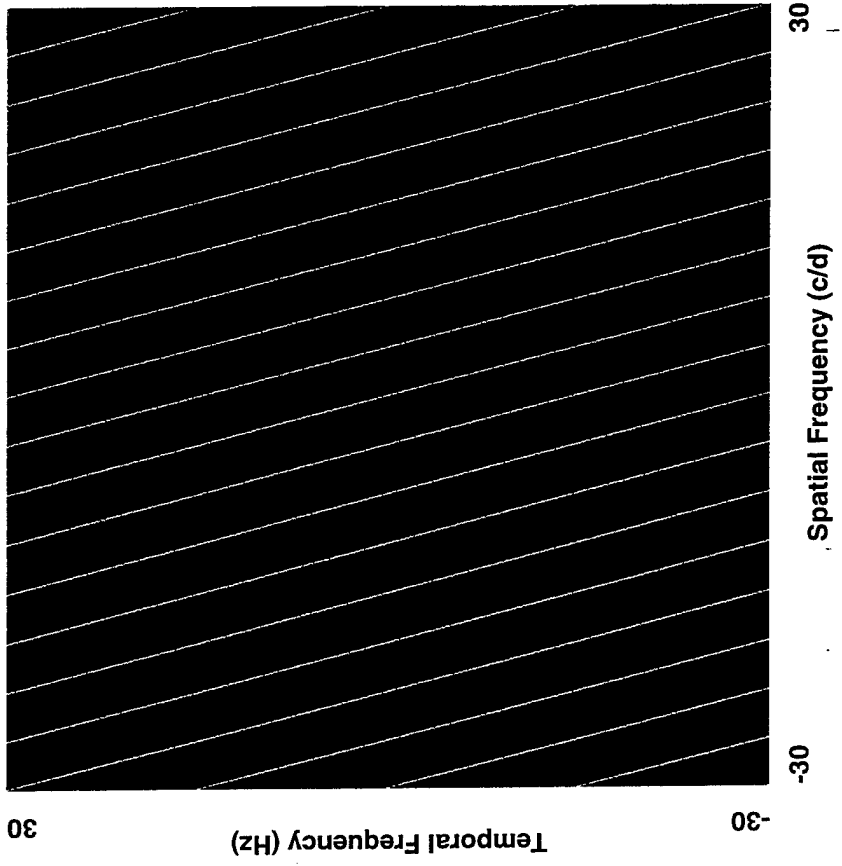
Figure 11

Spatiotemporal-frequency spectra. The left panel represents the spectrum of a motion sequence with a velocity of -4 deg/sec and a duration of 67 msec (4 target presentations). The right panel represents the spectrum of a sampling function in which the impulses are separated in time by 67 sec and in space by 0.267 deg. In both panels, the horizontal dimension represents horizontal spatial frequencies from -30 cycles/deg to 30 cycles/deg, and the vertical dimension represents temporal frequencies from -30 Hz to 30 Hz. The brightness of a point indicates its magnitude.
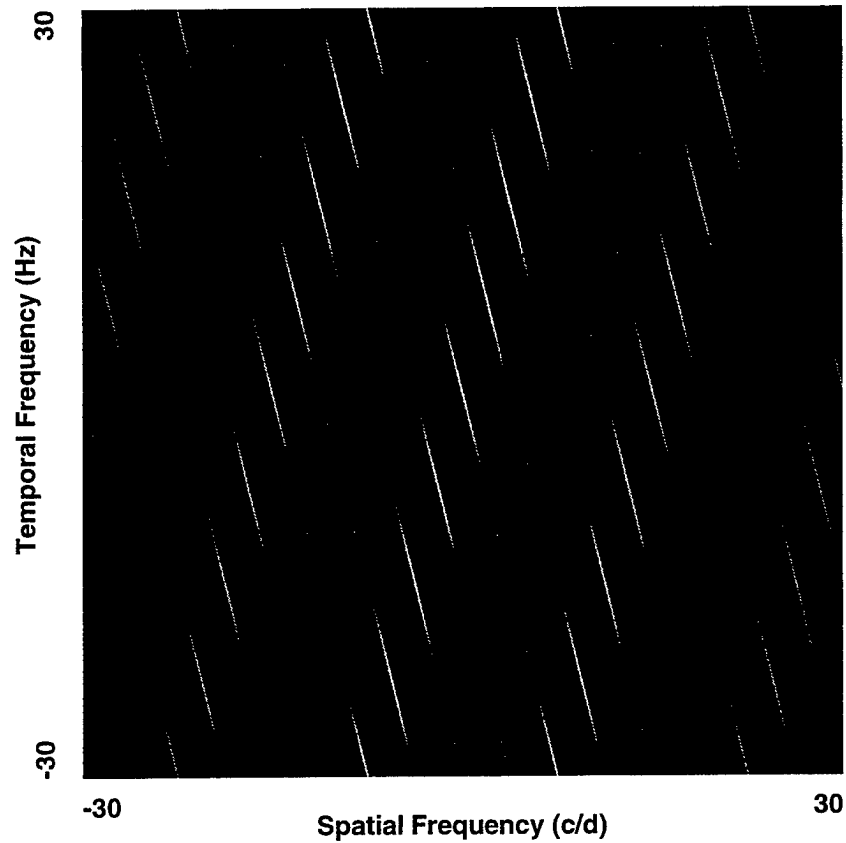
Figure 12

Spectrum of motion sequence with a global velocity of 4 deg/sec, a local velocity of -4 deg/sec, and a segment duration of 67 msec (4 target presentations). This spectrum represents the product of the spectra in Figure 11. The horizontal dimension represents horizontal spatial frequencies from -30 cycles/deg to 30 cycles/deg, and the vertical dimension represents temporal frequencies from -30 Hz to 30 Hz. The brightness of a point indicates its magnitude.

origin with a slope of -4 deg/sec define the set of sinusoidal components with a drift velocity of 4 deg/sec (i.e., in accord with the GV). Note that the GV is predominant for only a narrow band of spatial frequencies. Spatiotemporal frequencies in accord with the LV are present only where the lines in the spectrum of the sampling function "sliced" through the nonaliased energy in the spectrum of the single local-motion sequence. The remaining high-amplitude spatiotemporal-frequency components are consistent with neither velocity.

The component (Fig. 11) and composite (Fig. 12) spectra differ systematically for different values of GV, LV, and segment duration. The LV determines the slope, the number of bands of energy, and for a given segment duration, the spread along the spatial frequency dimension of the spectrum of a single segment. The effects of these differences on the spectra of the multisegment motion sequences are illustrated in Figures 13 and 14, which depict the spectra for sequences with a GV of 4 deg/sec and a segment duration of 67 msec, for LVs of -8, 0, 8, and 12 deg/sec. Note that the length of the central lobe of the constant velocity (GV) line is inversely proportional to the sawtooth speed.

Increasing the duration of a local-velocity segment decreases the spread of its spectrum. It also increases the spatiotemporal interval between impulses in the sampling function and thus decreases the spacing between replicas in its spectrum. As a result, in the spectrum of the multisegment motion sequence, the number of spectral components consistent with the GV decreases, and the number consistent with the LV increases. This effect is illustrated in Figure 15, which depicts the spectra for sequences with a GV of 4 deg/sec, an LV of -4 deg/sec, and segment durations of 200 msec (left panel) and 400 msec (right panel) .

For a GV of 0 deg/sec, the impulses in the sampling function were separated only in time. Therefore, the lines in the spectrum of the sampling function are horizontal and occur at $w = 0$ Hz and multiples of the temporal sampling rate. Figure 16 illustrates the spectra of multisegment motion sequences with a GV of 0 deg/sec, an LV of -8 deg/sec, and durations of 67 msec (left panel) and 200 msec (right panel). Note that, in both spectra, there are numerous spatial frequencies with a temporal frequency of zero (i.e., in accord with the GV) and that the other velocities more-or-less cancel each other out. A comparison of the right panel of Figure 16 and the left panel of Figure 15 suggests why the LV affected pursuit velocity at shorter segment durations for a GV of 4 deg/sec than for a GV of 0 deg/sec. Although both spectra represent a segment duration of 200 msec, the number of spectral components in accord with the LV is greater for GV4 than for GV0.

As was shown in Figures 12-14, GV motion was predominant for only a narrow band of spatial frequencies when the segment duration was 67 msec. This band decreased as segment duration increased. To assess the bandwidth for the longest segment duration at which there was no effect of the LV, we plotted the temporal frequency spectra of spatial frequencies up to 5 cycles/deg for each of the GV4 motion sequences with a segment duration of 133 msec. We used 256 x 256 point FFTs (with motion sequences of appropriately limited durations) and spatial- and temporal-sampling rates of 60 cycles/deg and 60 Hz, respectively. These spectra, which provided a spatial-frequency resolution of 0.23 cycles/deg, indicated that GV motion was
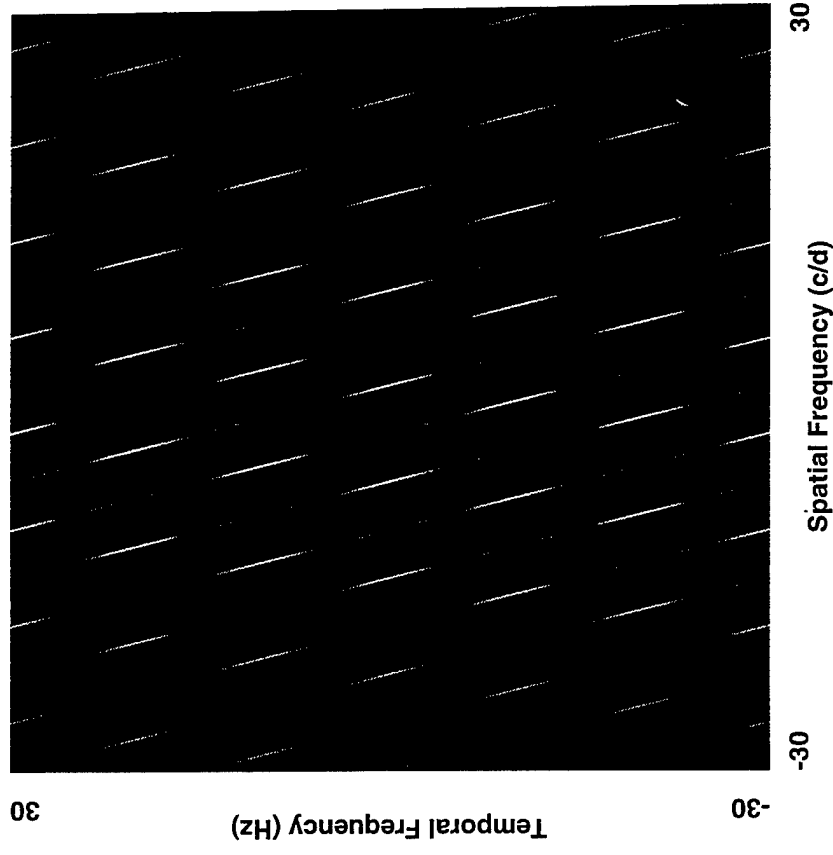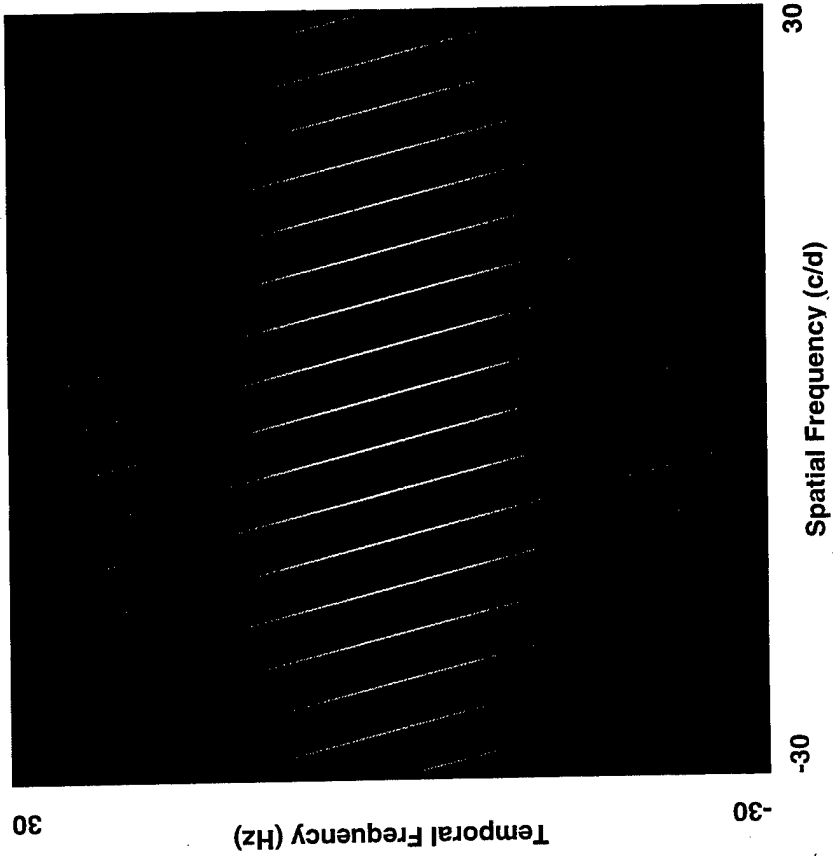
Figure 13

Spectra of motion sequences with a global velocity of 4 deg/sec, a segment duration of 67 msec, and local velocities of -8 deg/sec (left panel) and 0 deg/sec (right panel). The horizontal dimension represents horizontal spatial frequencies from -30 cycles/deg to 30 cycles/deg, and the vertical dimension represents temporal frequencies from -30 Hz to 30 Hz. The brightness of a point indicates its magnitude.

25
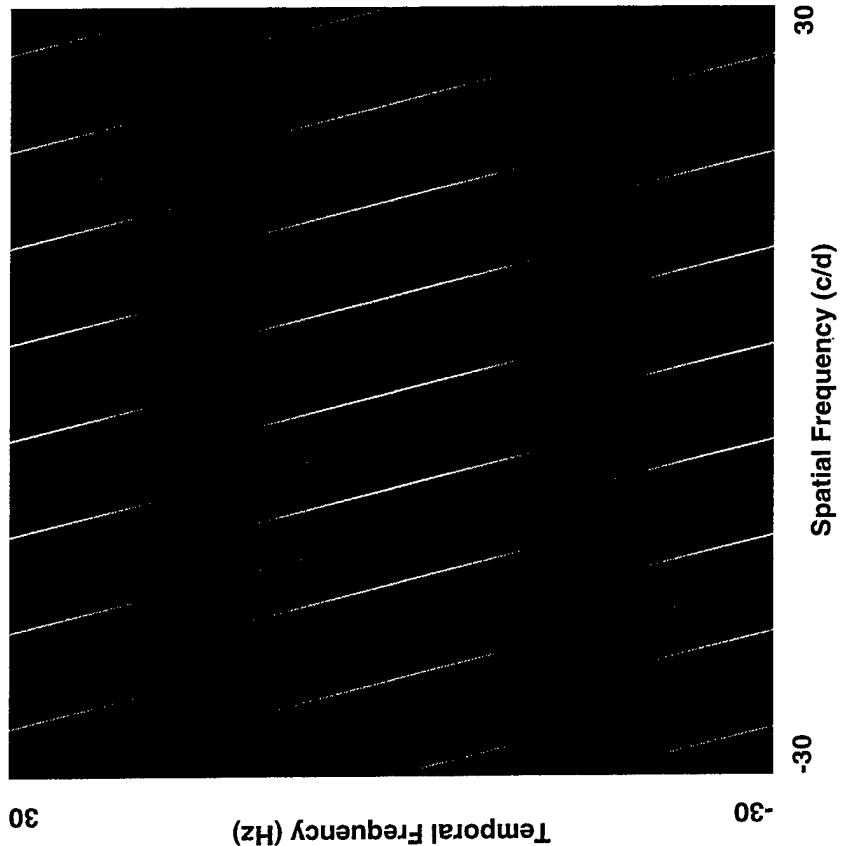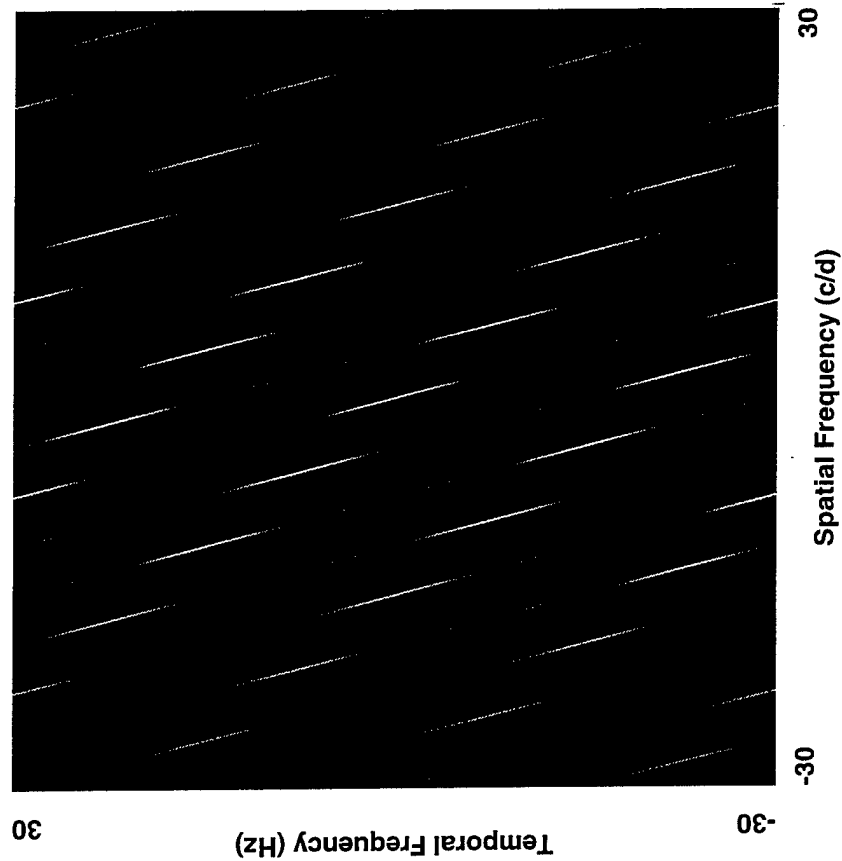
Figure 14

Spectra of motion sequences with a global velocity of 4 deg/sec, a segment duration of 67 msec, and local velocities of 8 deg/sec (left panel) and 12 deg/sec (right panel). The horizontal dimension represents horizontal spatial frequencies from -30 cycles/deg to 30 cycles/deg, and the vertical dimension represents temporal frequencies from -30 Hz to 30 Hz. The brightness of a point indicates its magnitude.
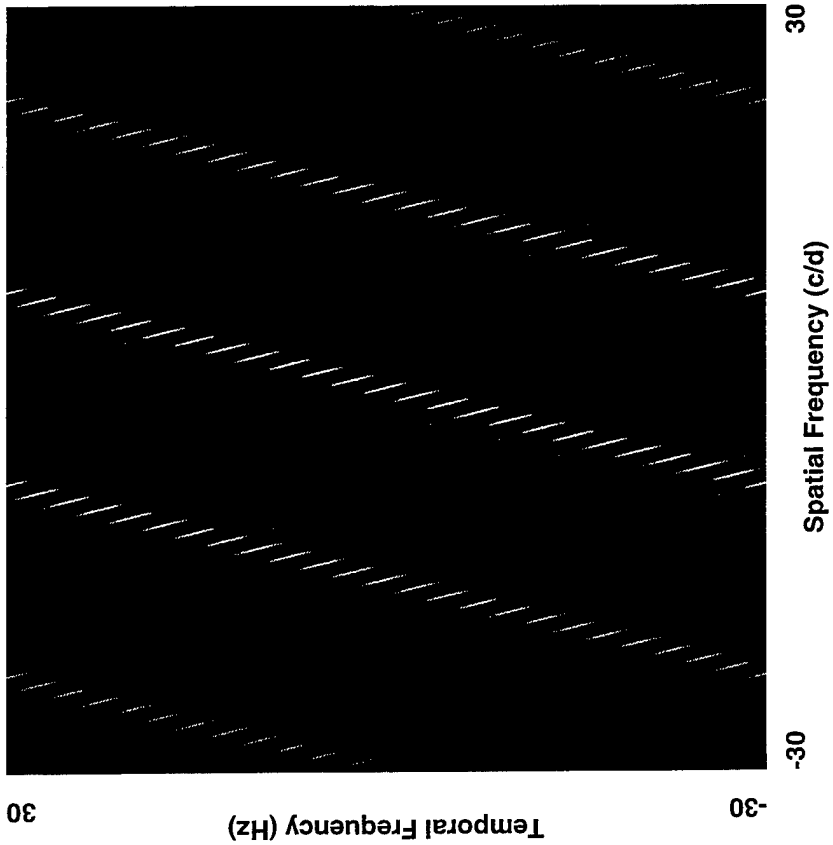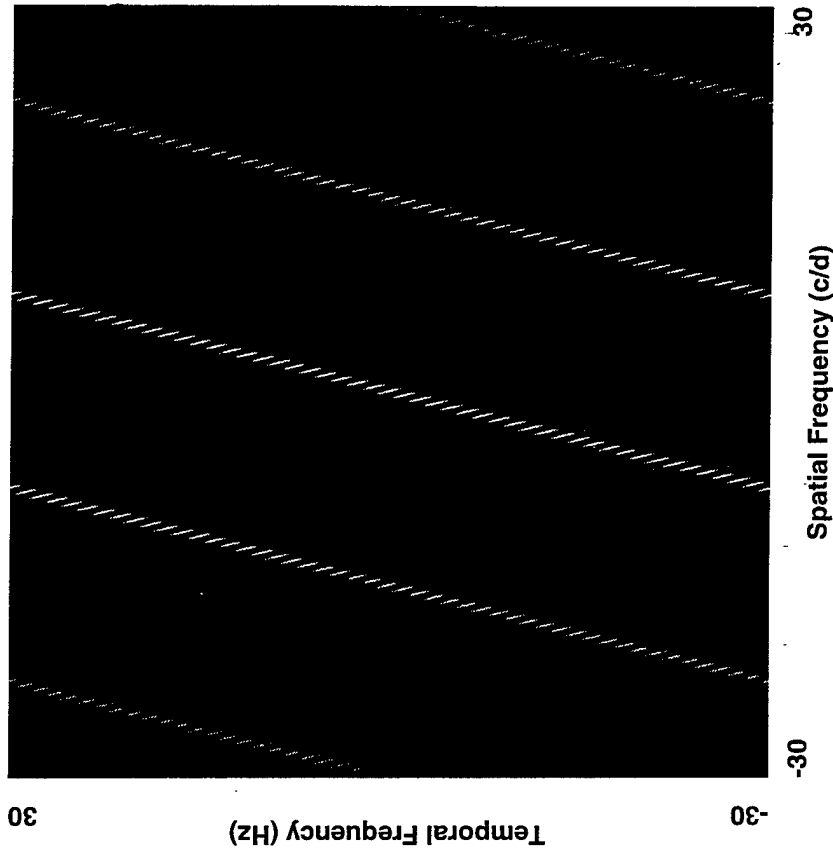
Figure 15

Spectra of motion sequences with a global velocity of 4 deg/sec, a local velocity of -4 deg/sec, and segment durations of 200 msec (left panel) and 400 msec (right panel). The horizontal dimension represents horizontal spatial frequencies from -30 cycles/deg to 30 cycles/deg, and the vertical dimension represents temporal frequencies from -30 Hz to 30 Hz. The brightness of a point indicates its magnitude.
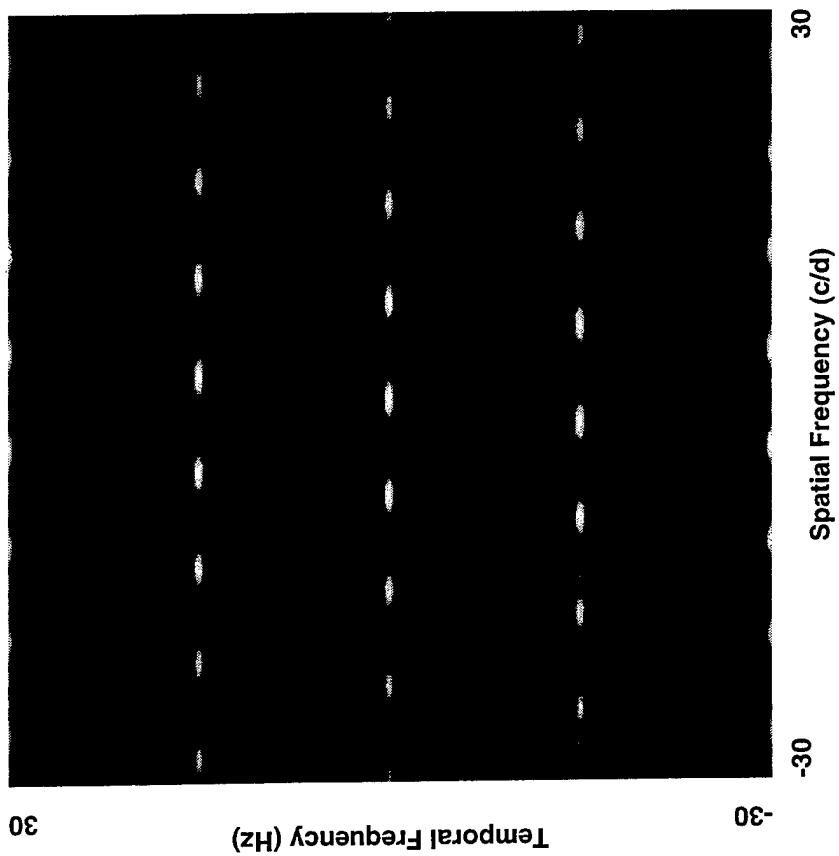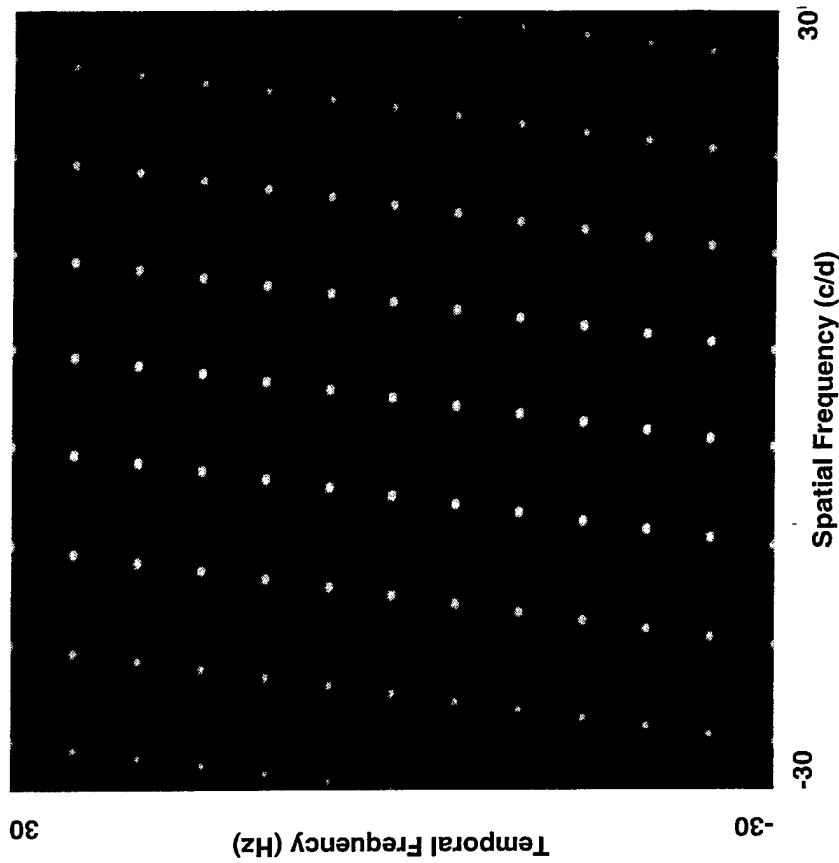
Figure 16

Spectra of motion sequences with a global velocity of 0 deg/sec, a local velocity of -8 deg/sec, and segment durations of 67 msec (left panel) and 200 msec (right panel). The horizontal dimension represents horizontal spatial frequencies from -30 cycles/deg to 30 cycles/deg, and the vertical dimension represents temporal frequencies from -30 Hz to 30 Hz. The brightness of a point indicates its magnitude.

consistently predominant, across LVs, only for the lowest spatial frequency sampled (i.e., 0.23 cycles/deg). The maximum spatial frequency at which the temporal-frequency spectrum was in accord with the GV increased as the sawtooth speed decreased.

Human observers can track drifting gratings with fundamental spatial frequencies well in excess of 0.23 cycles/deg. The data presented here do not indicate that sawtooth speed affected the duration at which the LV began to have an effect on pursuit velocity. Perhaps the pursuit system weights the velocity information provided by a given spatiotemporal-frequency component according to how well it matches the velocity specified by the lowest spatial frequencies: In the spectra of the multisegment motion sequences, the higher sawtooth speeds were characterized by fewer very low spatial frequencies but a greater number of higher spatial frequencies with a drift velocity equal to the GV (see Figs. 13 and 14). In any case, these multisegment motion sequences had very complex spectra, and the response of the pursuit system (up to a segment duration of about 167 msec) was very consistent. If the motion sensors for the pursuit system begin with a spatiotemporal filtering process, the velocity signal must be heavily dependent upon the velocities of very low spatial frequency components.

As segment duration increased, the spectrum of a multisegment motion sequence was decreasingly in accord with the GV and increasingly in accord with the LV (see Fig. 15). This spectral difference could, of itself, account for the gradual shift from a pursuit velocity in accord with the GV to a pursuit velocity in accord with the LV. However, without limiting the temporal window over which velocity computations occur, the shift toward a spectrum dominated by the LV is quite specific to our stimuli. It would not characterize composite waveforms formed by adding a constant velocity ramp and a high frequency waveform with equal motion in both directions--such as a sinusoid or a triangle. Nonetheless, Martins et al. (1985), who presented sinusoidal target motion, found a similar shift from global (i.e., 0 deg/sec) to local tracking as the period of the sinusoid increased. The size and shape of the temporal window for velocity computations is likely to be an important component of any adequate model of the motion sensor for the pursuit system.

Finally, there is the question of the stimulus for the maintenance of pursuit. During any period of constant-velocity smooth pursuit, the spatiotemporal frequency spectrum of the retinal image would be sheared with respect to the spectrum of the motion sequence: The temporal frequency of every spatiotemporal frequency component would be increased by the product of its spatial frequency and the velocity of the eye. If pursuit velocity were exactly matched to the GV of a motion sequence, the GV of the retinal image would equal 0 deg/sec and the LV of the retinal image would equal the STV. For example, during perfect tracking of the GV of a motion sequence with a GV of 4 deg/sec, an LV of -4 deg/sec, and a segment duration of 67 msec (Fig. 12), the spectrum of the resulting space-time retinal image would equal that of a motion sequence with GV 0f 0 deg/sec, an LV of -8 deg/sec, and a segment duration of 67 msec (left panel, Fig. 16).

Tracking of the GV was, of course, never perfect (see Fig. 3). To assess the effects of these imperfections, the space-time "retinal image" for a trial was calculated by subtracting each target position from the average of the ten samples of eye position for each frame of the motion sequence. For these calculations, the first target presentation was assumed to occur half a frame after the first eye-position sample.

Figure 17 illustrates the retinal-image spectra for trials in which the pursuit velocity was well matched to the GV. The left panel depicts the spectrum for a trial in which the GV was 0 deg/sec, the LV was -8 deg/sec, and the duration was 67 msec. The right panel depicts the spectrum for a trial in which the GV was 4 deg/sec, the LV was -4 deg/sec, and the duration was 67 msec. Note that these spectra are nearly identical: In each, high amplitudes are found for a narrow band of spatial frequencies (centered at 0 cycles/deg) with a temporal frequency near 0 Hz as well as for narrow bands of spatial frequencies near ± 15 Hz. The former are consistent with a velocity of about 0 deg/sec, the latter with a velocity of -8 deg/sec. The temporal frequencies for the higher spatial frequencies (see the left panel of Fig. 16) are spread over the temporal frequency space. Although pursuit in accord with the GV did not reduce retinal image motion to zero, it did stabilize the position of low spatial frequencies in the retinal image. It may be that pursuit is maintained not by the absence of retinal image motion but by the presence of appreciable spectral energy for components with a drift velocity of approximately zero.
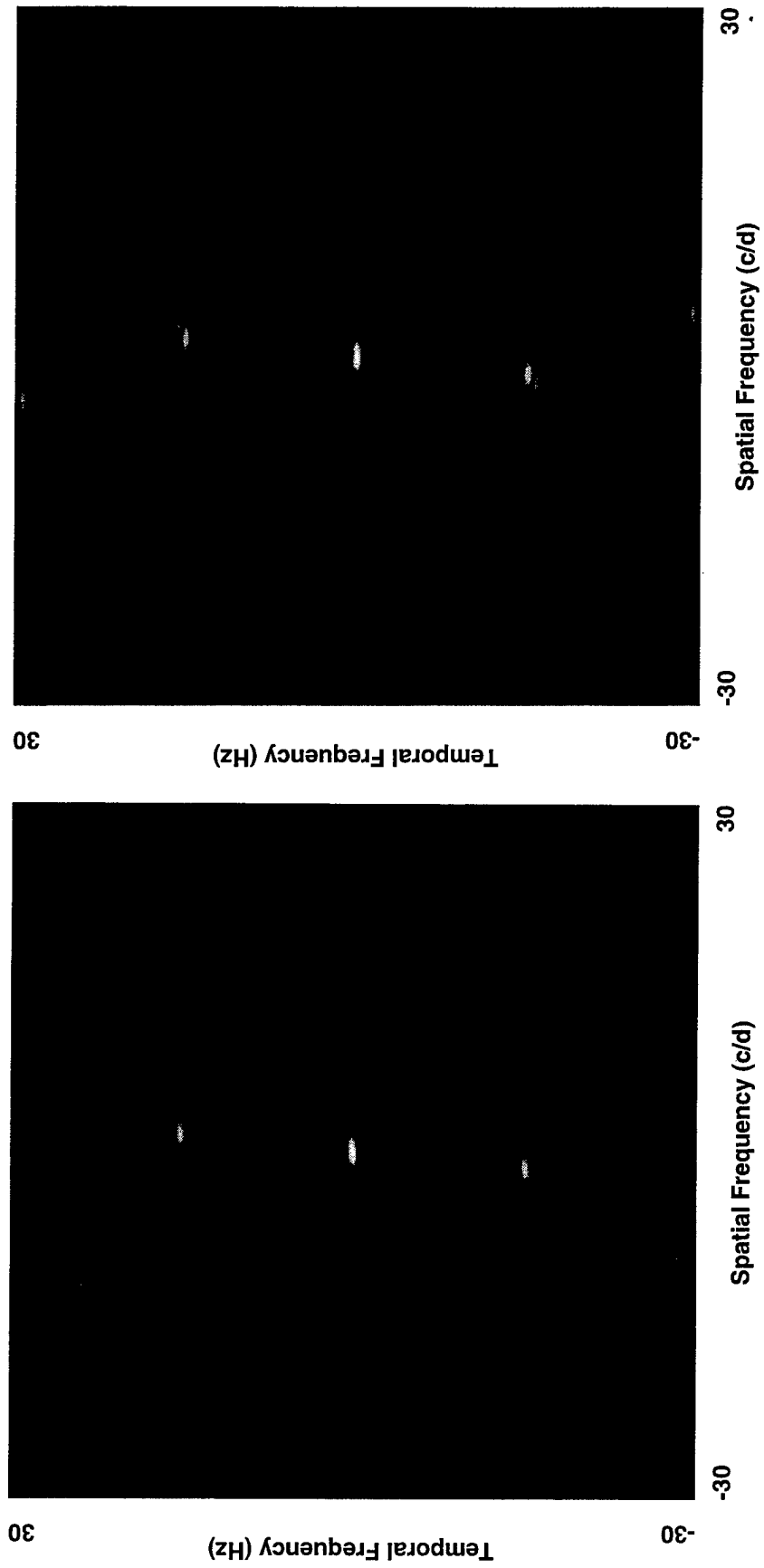
Figure 17

Spectra of retinal images formed during tracking in accord with the global velocity of motion sequences with a local-segment duration of 67 msec. The motion sequence for the left panel had a global velocity of 0 deg/sec and a local velocity of -8 deg/sec. The motion sequence for the right panel had a global velocity of 4 deg/sec, a local velocity of -4 deg/sec, and a sawtooth velocity of -8 deg/sec. The horizontal dimension represents horizontal spatial frequencies from -30 cycles/deg to 30 cycles/deg, and the vertical dimension represents temporal frequencies from -30 Hz to 30 Hz. The brightness of a point indicates its magnitude.

31

REFERENCES

Adelson, E. H., & Bergen, J. R. (1985). Spatiotemporal energy models for the perception of motion. *Journal of the Optical Society of America*, **A2**, 284-299.

Collewijn, H., & Tamminga, E. P. (1984). Human smooth pursuit and saccadic eye movements during voluntary pursuit of different target motions on different backgrounds. *Journal of Physiology*, **351**, 217-250.

Hallet, P. E. (1986). Eye movements. In K. R. Boff, L. Kauffman, & J. P. Thomas (Eds.), *Handbook of perception and human performance, Vol. 1*, Chapter 10. New York: Wiley.

Hempstead, C. F. (1966). Motion perception using oscilloscope display. *IEEE Spectrum*, 128-135.

Heywood, S. (1973). Pursuing stationary dots: Smooth eye movements and apparent movement. *Perception*, **2**, 181-195.

Kowler, E. (1989). Cognitive expectations, not habits, control anticipatory smooth oculomotor pursuit. *Vision Research*, **29**, 1049-1057.

Lamontagne, C., Desjardins, F. J., & Pivik, R. T. (1993). Smooth pursuit along a solid line: A new variation on the theme of efference-copy-bound eye tracking. *Perception*, **22**, 477-482.

Leigh, R. J., & Zee, D. S. (1991). *The neurology of eye movements* (2nd edition). Philadelphia: F. A. Davis Co.

Lindholm, J. M. (1991). Perceptual consequences of the filtering characteristics of the pursuit system. *Bulletin of the Psychonomic Society*, **29**, 477.

Lindholm, J. M. (1992a). Perceptual effects of spatiotemporal sampling. In M. A. Karim (ed.) *Electro-Optical Displays* (pp. 787-807). New York: Marcel Dekker.

Lindholm, J. M. (1992b). *Temporal and Spatial Factors Affecting the Perception of Computer-Generated Imagery*. AL-TR-1991-0140. Williams AFB, AZ: Operations Training Division, Air Force Human Resources Laboratory.

Lisberger, S. G., Evinger, C., Johanson, G. W., & Fuchs, A. F. (1981). Relationship between eye acceleration and retinal image velocity during foveal smooth pursuit in man and monkey. Journal of Neurophysiology, **46**, 229-249.

Lisberger, S. G., Morris, E. J., & Tychsen, L. (1987). Visual motion processing and sensory-motor integration for smooth pursuit eye movements. *Annual Review of Neuroscience*, **10**, 97-129.

Martins, A. J., Kowler, E., & Palmer, C. (1985). Smooth pursuit of small-amplitude sinusoidal motion. *Journal of the Optical Society of America*, **A2**, 234-242.

Morgan, M. J., & Turnbull, D. F. (1978). Smooth pursuit tracking and the perception of motion in the absence of real movement. *Vision Research*, **18**, 1053-1059.

Robinson, D. A., Gordon, J. L., & Gordon, S. E. (1986). A model of the smooth pursuit eye movement system. *Biological Cybernetics*, **55**, 43-57.

Stoper, A. (1973). Apparent motion of stimuli presented stroboscopically during pursuit eye movements. *Perception and Psychophysics*, **13**, 301-311.

van Santen, J. P. H., & Sperling, G. (1984). A temporal covariance model of motion perception. *Journal of the Optical Society of America*, **A1**, 451-473.

Watson, A. B., & Ahumada, A. J., Jr. (1985). A model of human visual-motion sensing. *Journal of the Optical Society of America*, **A2**, 1600-1606.

Young, L. R., (1971). Pursuit eye tracking movements. In P. Bach-y-Rita, C. C. Collins, & J. E. Hyde (Eds.), *Control of eye movements*, pp. 429-443. Amsterdam: Elsevier.